Received: 7 September 2018 | Accepted: 26 June 2019

DOI: 10.1002/hyp.13546

SPECIAL ISSUE CANADIAN GEOPHYSICAL UNION

WILEY

# Modelling the effects of permafrost loss on discharge from a wetland-dominated, discontinuous permafrost basin

Lindsay E. Stone[1] | Xing Fang[2] | Kristine M. Haynes[1] | Manuel Helbig[3,4] | John W. Pomeroy[2] | Oliver Sonnentag[4] | William L. Quinton[1]

[1]Cold Regions Research Centre, Wilfrid Laurier University, Waterloo, ON, Canada

[2]Centre for Hydrology, University of Saskatchewan, Saskatoon, SK, Canada

[3]School of Geography and Earth Sciences, McMaster University, Hamilton, ON, Canada

[4]Département de géographie and Centre d'études nordiques, Université de Montréal, Montréal, QC, Canada

**Correspondence**
Kristine M. Haynes, Cold Regions Research Centre, Wilfrid Laurier University, 75 University Avenue West, Waterloo, Ontario, N2L 3C5, Canada.
Email: khaynes@wlu.ca

**Funding information**
Natural Sciences and Engineering Research Council of Canada, Grant/Award Number: CRDPJ 469053 - 14; Natural Sciences and Engineering Research Council of Canada Climate Change and Atmospheric Research Initiative, Grant/Award Number: RGPCC - 433923-2012; Government of the Northwest Territories (GNWT); Northern Scientific Training Program; NSERC Changing Cold Regions Network (CCRN)

## Abstract

Permafrost degradation in the peat-rich southern fringe of the discontinuous permafrost zone is catalysing substantial changes to land cover with expansion of permafrost-free wetlands (bogs and fens) and shrinkage of forest-dominated permafrost peat plateaux. Predicting discharge from headwater basins in this region depends upon understanding and numerically representing the interactions between storage and discharge within and between the major land cover types and how these interactions are changing. To better understand the implications of advanced permafrost thaw-induced land cover change on wetland discharge, with all landscape features capable of contributing to drainage networks, the hydrological behaviour of a channel fen sub-basin in the headwaters of Scotty Creek, Northwest Territories, Canada, dominated by peat plateau–bog complexes, was modelled using the Cold Regions Hydrological Modelling platform for the period of 2009 to 2015. The model construction was based on field water balance observations, and performance was deemed adequate when evaluated against measured water balance components. A sensitivity analysis was conducted to assess the impact of progressive permafrost loss on discharge from the sub-basin, in which all units of the sub-basin have the potential to contribute to the drainage network, by incrementally reducing the ratio of wetland to plateau in the modelled sub-basin. Simulated reductions in permafrost extent decreased total annual discharge from the channel fen by 2.5% for every 10% decrease in permafrost area due to increased surface storage capacity, reduced run-off efficiency, and increased landscape evapotranspiration. Runoff ratios for the fen hydrological response unit dropped from 0.54 to 0.48 after the simulated 50% permafrost area loss with a substantial reduction of 0.47 to 0.31 during the snowmelt season. The reduction in peat plateau area resulted in decreased seasonal variability in discharge due to changes in the flow path routing, with amplified low flows associated with small increases in subsurface discharge, and decreased peak discharge with large reductions in surface run-off.

**KEYWORDS**

Cold Regions Hydrological Modelling platform, discharge, discontinuous permafrost, drainage network, flow paths, hydrological connectivity, land cover change, peatlands

 © 2019 John Wiley & Sons, Ltd. 

## 1 | INTRODUCTION

Northwestern Canada is experiencing rapid climate warming with air temperatures increasing at twice the rate of the global average (IPCC, 2014). Shallow permafrost temperatures have increased (Smith, Burgess, Riseborough, & Nixon, 2005; Taylor, Wang, Smith, Burgess, & Judge, 2006), resulting in widespread degradation and loss at an accelerating rate in the discontinuous and sporadic permafrost zones (Camill, 2005), including at the southern margin of the discontinuous zone of northwestern Canada (Kwong & Gan, 1994). Permafrost degradation has significant impacts on the hydrology of northern ecosystems. For example, studies have highlighted increasing baseflow across the Northwest Territories (St. Jacques & Sauchyn, 2009), changes in the rate of catastrophic lake drainage (Marsh, Russell, Pohl, Haywood, & Onclin, 2009), and widespread land cover changes with thermokarst development as surface vegetation transitions from boreal forest to extensive wetlands (Jorgenson, Racine, Walters, & Osterkamp, 2001; Quinton, Hayashi, & Chasmer, 2009). Changes in the hydrology affect other key ecosystem processes such as carbon dynamics (Dimitrov, Bhatti, & Grant, 2014; Helbig et al., 2017; O'Donnell et al., 2012), transport of nutrients (Frey & McClelland, 2009) and toxins (Gordon, Quinton, Branfireun, & Olefeldt, 2016), and ground thermal regimes (Sjöberg et al., 2016).

The impact of permafrost degradation and ultimately loss in the discontinuous permafrost region is tightly linked to dramatic landscape and ecological change. Black spruce-dominated peat plateaux are raised by 1–2 m above the surrounding wetlands due to an ice-rich permafrost core (Quinton, Hayashi, & Pietroniro, 2003). When this permafrost core thaws, the ground surface subsides and is flooded by the adjacent wetlands (thermokarst bog or fen). Waterlogging along the edge of thawing permafrost causes decreased root activity under anaerobic conditions (Kozlowski, 1984), eventually leading to reduced black spruce tree cover and a transition from forest to wetland (Baltzer, Veness, Chasmer, Sniderhan, & Quinton, 2014; Patankar, Quinton, Hayashi, & Baltzer, 2015). As permafrost thaw proceeds, the characteristic run-off generation function of peat plateaux is reduced resulting from the transition to wetland and the loss of the hydraulic gradient between peat plateau and adjacent bog or fen (Quinton & Baltzer, 2013). Channel fens convey run-off to the basin outlet (Hayashi, Quinton, Pietroniro, & Gibson, 2004), whereas bogs have been considered storage features in the landscape (Quinton et al., 2003). However, breaches in permafrost surrounding bogs has increased wetland hydrological connectivity and facilitated the exchange of water between adjacent bogs as well as between bogs and channel fens, contributing run-off to drainage networks (Connon, Quinton, Craig, Hanisch, & Sonnentag, 2015; Connon, Quinton, Craig, & Hayashi, 2014; Haynes, Connon, & Quinton, 2018). A change in the relative proportion of bog, fen, and peat plateau area in a basin influences the basin hydrograph, with increased run-off from discontinuous permafrost watersheds attributed to the thaw-induced increase in run-off contributing area and transient contributions of wetland drainage (Connon et al., 2014; Haynes et al., 2018).

Predicting basin discharge along the southern margin of permafrost distribution in northwestern Canada depends upon an understanding of the individual impacts of permafrost degradation on the major land cover types and their hydrological interactions. Substantial improvements have been made in understanding the hydrological contributions from peat plateaux (Quinton & Baltzer, 2013; Quinton & Hayashi, 2008) and bogs (Connon et al., 2015; Haynes et al., 2018) to channel fens with continued permafrost degradation. Despite the functional understanding of fens as lateral transport features conveying water to the basin outlet (Quinton et al., 2003) and the application of roughness-based algorithms for approximating surface discharge (Hayashi et al., 2004), the mechanisms by which channel fens store and transport water are not well understood. An improved understanding of the hydrological functioning of channel fens is needed to inform numerical modelling of fen discharge and to accurately assess how fen discharge might be altered by climate and other environmental changes in northwestern Canada and other similar high-latitude regions. Examination of a detailed water balance, combined with previous works on the hydrological mechanisms governing bog cascades (e.g., Connon et al., 2015) and peat plateaux (e.g., Wright, Hayashi, & Quinton, 2009), will facilitate more accurate representation of the fen–bog–plateau complexes, characteristic of the discontinuous permafrost zone, in numerical models. Additionally, previous studies on permafrost degradation in this region examined the hydrological impacts of expanding run-off contributing areas through thaw-induced increases in hydrological connectivity (e.g., Chasmer & Hopkinson, 2016; Connon et al., 2014). However, it has been suggested that permafrost thaw-induced landscape change will over time exhibit a diminishing return on basin discharge as the upper limit of hydrological connectivity is approached (Haynes et al., 2018). The influence of these anticipated changes on the hydrology of channel fens requires further study.

This study aims to improve the mechanistic understanding of how permafrost thaw-driven conversion of forest to wetland affects the hydrology of channel fens. This will be achieved through the following objectives: (a) develop a conceptual model illustrating the seasonally dominant hydrological processes governing the water balance of a channel fen sub-basin using field hydrometric measurements; (b) develop and evaluate the performance of a numerical model of the discharge from a channel fen sub-basin, with all adjacent land cover types able to contribute to the drainage network, using the Cold Regions Hydrological Modelling (CRHM) platform; and (c) assess the sensitivity of modelled channel fen sub-basin discharge to the incremental loss of permafrost and the concomitant increase in the area of permafrost-free bog and channel fen land cover.

## 2 | STUDY SITE

The Scotty Creek watershed (152 $km^2$) is located in the high boreal ecoregion in the lower Liard River valley, Northwest Territories, Canada. The basin is in the southern fringe of the discontinuous permafrost zone, approximately 50 km south of Fort Simpson (Figure 1a,

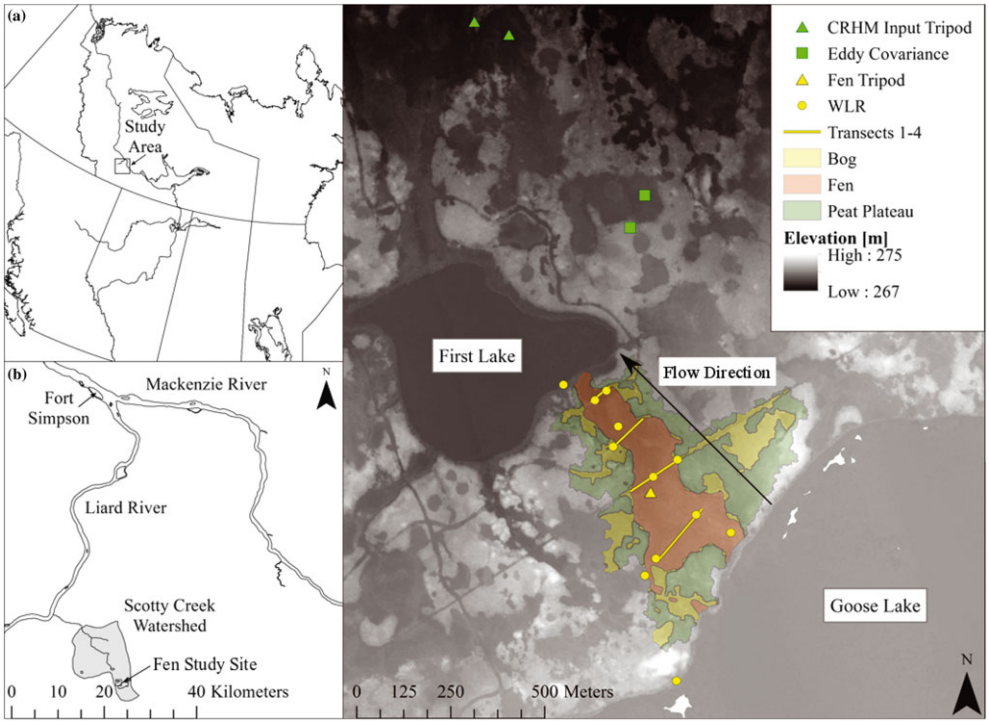


**FIGURE 1** (a) Study area within the Northwest Territories, (b) the Scotty Creek basin, and (c) the studied channel fen (red) including land cover types, equipment locations, and elevation from Light Detection and Ranging survey. Equipment locations (e.g., eddy covariance and meteorological tripods) in green were used for numerical modelling in Cold Regions Hydrological Modelling platform (CRHM) and performance evaluation. Equipment locations (e.g., water level recorders, and meteorological tripod) within the channel fen watershed in yellow were part of the water balance calculations performed to develop the conceptual model

b). Approximately 40% of the basin is underlain by shallow permafrost (<10 m thick; Burgess & Smith, 2000; Quinton, Hayashi, & Chasmer, 2011). Daily average air temperature (1981–2010) recorded at the Fort Simpson airport is −2.8°C, with average air temperatures of −24.2°C for January and 17.4°C for July. The region receives an average of 388 mm of precipitation annually, of which 187 mm falls as snow (Environment and Climate Change Canada, 2017). Elevation in the basin ranges from 210 to 285 m above sea level, with an average gradient of 0.0032 m/m (Quinton & Hayashi, 2008). The majority of the basin has deep peat deposits (2–8 m) underlain by a clay-rich glacial till with occasional sandy mineral uplands (Aylsworth et al., 2000; McClymont, Hayashi, Bentley, & Christensen, 2013).

The headwater portion of the Scotty Creek basin is characterized by large wetland areas interspersed with raised, forested peat plateaux and small lakes (Quinton et al., 2003). There are four major land cover types in this portion of the basin: peat plateau, channel fen, bog, and lake. In the Scotty Creek basin, the areal portion of land cover types is approximately 20% peat plateau, 12% fen, 19% bog, and 3% lake, with 43% of the area as mineral uplands, which are absent from the wetland-dominated headwaters (Chasmer, Hopkinson, Veness, Quinton, & Baltzer, 2014; Quinton & Hayashi, 2008). The basin headwaters area has seen a rapid decrease in permafrost area; 38% of peat plateau area was converted to wetlands between 1947 and 2008 (Quinton et al., 2011).

This study focuses on one channel fen sub-basin in the headwaters of the Scotty Creek basin that covers a straight distance of approximately 600 m between a source lake (Goose Lake) and outlet lake (First Lake, Figure 1c). The fen has well-defined edges with a limited number of hydrologically connected contributing areas including peat plateaux, bogs, and two linear disturbances (a cut line from seismic exploration and an abandoned winter road). Peat depth in the fen ranges between 3.0 to 4.5 m and is underlain by clay-rich glacial till with a relatively low hydraulic conductivity (Aylsworth et al., 2000; Aylsworth & Kettles, 2000).

## 3 | METHODS

### 3.1 | Field water balance

Four observation transects (identified as T1 through T4, Figure 1c) were established in late August 2014 that cross the fen surface perpendicular to the direction of flow in order to repeatedly sample snow depth and density, water depth and velocity, and depth to seasonal frost. All variables were measured approximately every 5 m along each transect, except for snow density that was measured every 25 m. Transects are separated by an average of 140 m with total distances of 175, 140, 105, and 65 m for Transects 1 through 4, respectively (see Figure 1c). Transects were oriented such that all characteristic vegetation types on the fen were included when sampling snow, water, and frost variables as well as extending into open connected features on each transect. In early March 2015, two ablation stakes were established along each of the four transects, one in an area representing the channel fen and one representing an open connected feature. The ablation stake data were supplemented with snow depth and density surveys along the transects conducted three times weekly at the end of the snow accumulation season and throughout the spring freshet to establish the rate of snowmelt. Once the snow cover on the fen was depleted, water depth and velocity were monitored three times weekly using an acoustic Doppler system (SonTek, FlowTracker, San Diego, CA, USA) until water velocities were

below the detection limit. The depth of seasonal frost was monitored post-snowmelt using a frost probe at all transect points weekly during the first month after snowmelt or until the seasonal frost had disappeared. The location and elevation of all transect points and equipment was recorded using a differential Global Positioning System (dGPS, GS10 RTK GPS, Leica Geosystems, St. Gallen, Switzerland) with an orthometric datum.

Measurements of water level, snowmelt, rainfall, and evapotranspiration from the fen ($ET_{fen}$) were used to compute a channel fen water balance over the period of September 2, 2014 to August 26, 2015 (Equation (1)). Four distinct time periods were assigned to examine seasonal differences in the water balance and are described in Table 1. Construction of the water balance was done by partitioning fluxes into three components: discharge into the fen, discharge out of the fen, and the atmospheric flux:

$$\Delta S = (Q_{sub}IN + Q_{sur}IN) - (Q_{sub}OUT + Q_{sur}OUT) + (P_r + P_s - ET), \quad (1)$$

where $\Delta S$ (mm day$^{-1}$) is the change in storage in the channel fen, $Q$ (mm day$^{-1}$) is the discharge of water into or out of the fen calculated separately for the surface discharge (sur) and the subsurface discharge (sub), $P_s$ (mm day$^{-1}$) is snowmelt added at the fen surface, $P_r$ (mm day$^{-1}$) is rainfall, and $ET$ (mm day$^{-1}$) is loss to the atmosphere through $ET_{fen}$. Incoming flow was calculated as the input into the channel fen from Goose Lake, as well as the input of the bog connected on T1, the seismic line connected on T2, the small bog connected on T3, and the winter road connected on T4 (Figure 1c). Outgoing discharge was the output from the channel fen to First Lake. Due to the low hydraulic conductivity of the underlying glacial till layer, deep groundwater flow was considered to be a net zero flux, with no vertical loss or gain (Connon et al., 2014). Surface discharge was calculated as a flux between two water level recorders using Manning's formula:

$$Q_{sur} = \frac{1}{n} A R_h^{\frac{2}{3}} S^{\frac{1}{2}}, \text{where for } w \gg d, R_h = d. \quad (2)$$

The cross sectional area, $A$ (m$^2$), is the width of the fen multiplied by the depth of water above the surface at the location of the upstream water level recorder. The hydraulic radius, $R_h$ (m), was approximated using the depth of water above the surface of the upstream water level recorder, as the fen width is significantly larger than the water depth. The slope of the water surface between the upstream and downstream water level recorder was calculated using dGPS elevation of the underlying wetland surface and adding the height of the water table above the fen surface and dividing by the straight line distance between the water level recorders. Manning's roughness coefficient, $n$ (s m$^{-1/3}$), was calculated by rearranging Manning's equation and using a velocity derived from the measured celerity, $c$ (m s$^{-1}$), in response to a large summer rain event.

$$n = d^{\frac{2}{3}} S^{\frac{1}{2}} \frac{5}{3c} \quad (3)$$

Average discharge rates for each 30-min interval were summed to obtain total daily surface discharge. The daily discharge was then divided by the surface area of the fen that was derived from a land cover classification map of the basin (Chasmer et al., 2014) to obtain the daily flux, $Q_{sur}$ (mm day$^{-1}$).

Subsurface discharge was calculated only for the saturated layer below the water table using Darcy's Law,

$$Q_{sub} = kA \frac{h_1 - h_2}{L}, \quad (4)$$

where the area, $A$ (m$^2$), is the width of the fen multiplied by the depth of saturated peat at the location of the downstream water level recorder. The depth of saturated peat is the distance between the full depth of the peat profile, as determined by field sampling, and the top of the saturated layer as recorded by the water level recorder. The hydraulic head, $h$ (m), was determined using the dGPS-measured elevation at the location of the water level recorder added to the depth of water relative to the surface. The distance between water level recorders, $L$ (m), was determined using dGPS location. The saturated hydraulic conductivity of a channel fen, $k$ (m s$^{-1}$), was determined to

**TABLE 1** Seasonal date periods for discussion of annual water balance

| Name | From date | To date | Reasoning |
|---|---|---|---|
| "Spring" | 04/04/2015 | 31/05/2015 | The first observation of snowmelt in the channel fen during field studies and ending when the water level in the fen reached a relatively stable height of within 5 cm above the fen surface |
| "Summer" | 01/06/2015 | 26/08/2015 | The time period after water table stabilization that occurred with the end of the spring freshet and ending when data collection ended in 2015 |
| "Fall" | 02/09/2014 | 17/12/2014 | The beginning of data recording and ending with the first recorded observation of ground temperature below 0 at the bog tripod (temp probe installed at 10 cm below the vegetated surface) |
| "Winter" | 18/12/2014 | 04/03/2015 | The remaining time interval between previously defined "fall" and "spring" |

have the following relationship with the depth from peat surface from field fen tracer tests conducted in the years 2000, 2003, and 2005 (Hayashi & Quinton, 2005).

$$k = 0.7701e^{3.8342d_p} \quad (5)$$

An average saturated hydraulic conductivity was calculated by taking the integral of the above relationship over the depth of saturated peat. The average half hourly discharge was summed to a daily flux, $Q_{sub}$ (mm day$^{-1}$), using the same method as that of surface discharge.

## 3.2 | Instrumentation

### 3.2.1 | Storage

A water level recorder network ($n$ = 12, Solinst Levelogger Gold, Solinst Canada, Georgetown, ON; Hobo U20L-04, Onset Computer Corporation, Bourne, MA, USA) was installed in the centre of the channel fen (Figure 1c) as well as in all non-forested connected land cover types (for example, bogs and linear disturbances) in late August 2014, recording every minute and calculating averages every 30 min. This water level recorder network was operational over winter 2014–2015, as it was installed significantly below freezing depths (>1 m). Water level recorders were anchored to a black iron pipe, which had been hammered into the underlying mineral soil to prevent mire breathing from moving the sensors (Fritz, Campbell, & Schipper, 2008). Measurements of depth to water table and depth to ground surface from the top of the well casing were collected at sensor installation and removal to establish water table position in reference to the ground surface and to confirm the lack of vertical well movement.

### 3.2.2 | Precipitation

Hourly total precipitation data were recorded using a weighing gauge (T-200B, Geonor, Augusta, NJ, USA) installed in August 2008 with no overhead canopy. Weighing gauge data were postprocessed using R statistical software (R Core Team, 2017) and the CRHMr R package (Shook, 2016) to correct recorded jitter (Pan et al., 2016). Precipitation data were then corrected for undercatch by determining precipitation type from hydrometeor temperature and adjusting for the catch efficiency of the gauge depending on wind speed measured at the height of the altar shield (Harder & Pomeroy, 2014; Smith, 2007).

### 3.2.3 | Evapotranspiration

In April 2015, a meteorological tripod was set up in a central location on the fen (equipment described in Table 2) to measure $ET_{fen}$ as input to the water balance. Fen evapotranspiration was measured using the high-frequency eddy covariance technique (Figure 1c, Krypton hygrometer and sonic anemometer, more details in Table 2), taking atmospheric water vapour and three-dimensional wind velocity measurements at a frequency of 10 Hz between April 9, 2015 and August 25, 2015. Latent heat fluxes were calculated using the EddyPro software (version 6.1.0; LI-COR Biosciences, Lincoln, NE, USA). Eddy covariance data processing included the following steps: the sonic anemometer tilt was corrected using double rotation, spikes were removed in the high-frequency time series using the method developed by Vickers and Mahrt (1997), high-frequency $ET_{fen}$ data were block averaged for an hourly time series, covariance maximization was used to compensate for time lags (Fan, Wofsy, Bakwin, Jacob, & Fitzjarrald, 1990), and the data quality was assessed for appropriate use in water budgets (Mauder & Foken, 2006). Applying the Webb-Pearman-Leuning, term accounted for water vapour density fluctuations (Webb, Pearman, & Leuning, 1980) and spectral attenuation due

**TABLE 2** Description of field instrumentation, location, and use in either the water balance or model

| Variable | Manufacturer details | Use | Equipment location |
|---|---|---|---|
| Water level | Solinst Levelogger Gold, HOBO U20 L-04 | Water balance | Fen |
| Four-component radiation | CNR4, Kipp and Zonen, the Netherlands | Water balance | Fen |
| Air temperature and relative humidity | HC-S3-XT, Rotronic Hygroclip, Switzerland | Water balance | Fen |
| Wind speed | 05103, R.M. Young, USA | Water balance | Fen |
| Depth to snow surface | SR50, Campbell Scientific Canada, AB | Water balance | Fen |
| Ground temperature | 109, Campbell Scientific Inc, USA | Water balance | Fen |
| 3-D wind velocity | CSAT, Campbell Scientific Inc, USA | Water balance | Fen |
| Water vapour flux | KH20, Campbell Scientific Inc, USA | Water balance | Fen |
| Incoming shortwave radiation | CNR1, Campbell Scientific Inc, USA | CRHM | Bog, Plateau |
| Air temperature and relative humidity | HMP45C, Vaisala Inc, Finland | CRHM | Bog, Plateau |
| Wind speed | 031A, Campbell Scientific Inc, USA | CRHM | Bog, Plateau |
| Depth to snow surface | SR50, Campbell Scientific Inc, USA | CRHM | Bog, Plateau |
| Water level | WL16s, Global Water Instrumentation, USA | CRHM | Bog |

Abbreviation: CRHM, Cold Regions Hydrological Model.

to sensor path length and separation was corrected according to Horst (1997) and Massman (2000). The source area of the $ET_{fen}$ measurements covers the main vegetation cover types of the study fen (i.e., herbaceous vegetation including cover of *Eriophorum* and *Carex* spp. with *Triglochin maritima* and *Menyanthes trifoliata*).

On days for which eddy covariance data were not available, the Priestley–Taylor (Priestley & Taylor, 1972) method was used to estimate $ET_{fen}$ from the fen surface. If less than 75% of hourly block-averaged eddy covariance data were available, then the Priestley–Taylor method was used to estimate daily $ET_{fen}$. During the "winter" period between December 18, 2014, and March 4, 2015, $ET_{fen}$ is assumed to be 0.

### 3.3 | Numerical model description—CRHM

CRHM is a flexible, physically based, modular modelling platform (Pomeroy et al., 2007). It uses the hydrological response unit (HRU) concept to permit flexible basin discretization from lumped to finely distributed and requires continuous forcing data including temperature, relative humidity, wind speed, and precipitation. A library of modules is available to model hydrological processes, with a focus on processes crucial to cold regions (e.g., blowing snow transport, interception, sublimation and melt, infiltration into frozen soils, ground freeze, and thaw). A basin-specific model application is built by selecting appropriate modules based on the basin of interest. Modules are parameterized using field observations, literature values, or by calibration. CRHM has been successfully applied to simulate hydrological processes across numerous cold regions locations (e.g., Fang et al., 2010; Fang et al., 2013; Krogh & Pomeroy, 2018) and to assess the sensitivity of these processes to climate and other environmental changes (e.g., Fang & Pomeroy, 2016; López-Moreno, Pomeroy, Revuelto, & Vicente-Serrano, 2012).

CRHM was used to model the hydrology of a small sub-basin (0.45 $km^2$) representative of the peat plateau–bog–channel fen complex located in the basin headwaters. Model modules were selected from those available to reflect, as closely as possible, the cold region processes governing the hydrology of this sub-basin that were identified in the conceptual model that was constructed based on field observations. The modules outlined in Figure 2 were chosen to represent the processes in this sub-basin, and further details of each module are provided in Table 3. The modelled sub-basin represents the hydrology of the channel fen that connects Goose Lake and First Lake (Figure 1c). The sub-basin area for the channel fen was determined through spatial analysis using the ArcMap Spatial Analyst/Hydrology toolbox using the 2010 LiDAR-derived digital elevation model (DEM) as input (Chasmer, Hopkinson, & Quinton, 2010). Due to the low topographic gradients of the headwaters of the Scotty Creek basin, there is little difference in slope, elevation, or aspect across the modelled sub-basin. Land cover type has been shown to be the most important factor driving the hydrological function in this basin (Quinton et al., 2003). The HRUs for the modelled sub-basin were determined from a land cover classification map of the Scotty Creek watershed based on 2010 LiDAR data collection (Chasmer et al., 2014). Therefore, the baseline model run is representative of the 2010 permafrost extent, covering 112,600 $m^2$ or 25% of the modelled sub-basin area.

Four HRUs were defined in this model: peat plateau, bog, fen, and lake. For the purpose of this study, all bogs within the sub-basin of the channel fen are considered hydrologically connected to the channel fen and the entire modelled sub-basin is considered to be a contributing area. This hydrological connectivity is modelled by the Muskingum routing module (Chow, 1964), which routes flow between HRUs within the sub-basin (Fang et al., 2010). As the overarching objective of this study was to simulate an advanced stage of permafrost thaw-induced landscape transition, this routing module was applied to model a fully connected system, with all sub-basin land cover types capable of contributing run-off to the drainage network, as is anticipated with permafrost loss (Haynes et al., 2018). The model simulates snow interception and sublimation from forest canopies, energy balance snowmelt, evapotranspiration, peat soil water storage and transmission, frost table dynamics, and run-off by surface, subsurface, and groundwater flows above the clay-rich layer. The selection of model parameters was informed by field observations conducted for this study, spatial analysis of the 2010 LiDAR-based digital

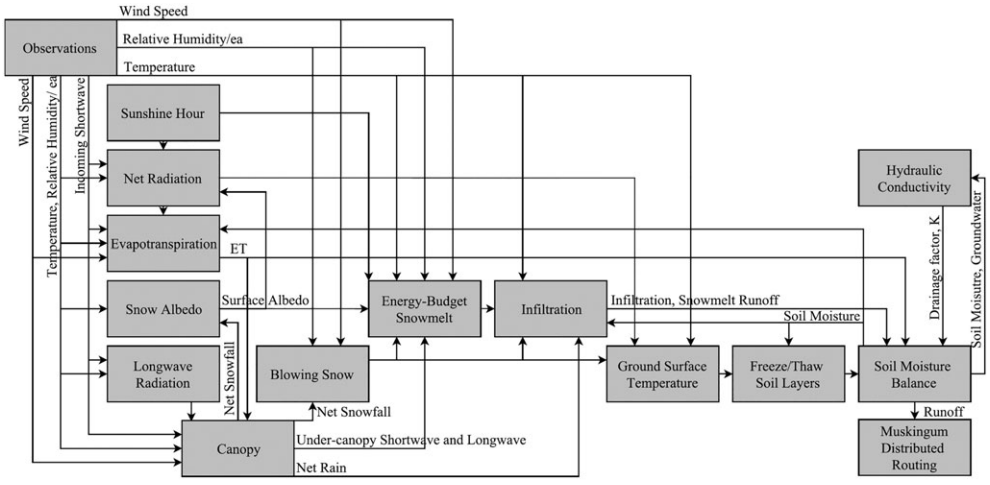


**FIGURE 2** Cold Regions Hydrological Modelling platform modules used to model physical processes of the subarctic muskeg. Lines indicate workflow

**TABLE 3** Description of Cold Regions Hydrological Modelling platform modules selected to model the channel fen

| Modules (module name and variation number) | Description |
|---|---|
| 1. Observations (obs): | Makes input meteorological data (wind speed, temperature, relative humidity, incoming shortwave radiation, and precipitation) available to other modules |
| 2. Sunshine hour (calcsun#1): | Uses incoming shortwave radiation to estimate sunshine hours; used as input to net all-wave radiation and snowmelt modules |
| 3. Longwave radiation (longVt): | Uses incoming shortwave radiation to calculate incoming longwave radiation; used as input to canopy module (Sicart, Pomeroy, Essery, & Bewley, 2006) |
| 4. Net radiation (netall): | Calculates the snow-free net all-wave radiation from the estimated shortwave radiation (Garnier & Ohmura, 1970) and the estimated net longwave radiation (Brunt, 1932) using air temperature, vapour pressure, and actual sunshine hours (Granger & Gray, 1990); used as input to evapotranspiration and ground surface temperature modules |
| 5. Evapotranspiration (evap_Resist): | Uses Priestley–Taylor evaporation equations (Priestley & Taylor, 1972) to calculate evaporation from saturated surfaces (wetlands and lake) and uses Penman–Monteith evaporation equations (Monteith, 1965) to calculate actual evaporation from the soil column in HRUs with unsaturated surfaces (peat plateau) |
| 6. Canopy (CanopyClearingGap#1): | Estimates the subcanopy shortwave and longwave radiation and canopy interception of snowfall and rainfall and updates under-canopy snowfall and rainfall. The module has options for a full forest canopy, a forest clearing gap, or a completely open area with no canopy effects (Ellis, Pomeroy, Brown, & MacDonald, 2010) |
| 7. Snow albedo (albedo_Richard): | Calculates snow albedo during winter and melt periods (Verseghy, 1991); used as input to energy budget snowmelt module |
| 8. Blowing snow (pbsm): | Simulates snow sublimation and transport between HRUs on the basis of surface aerodynamic roughness (Pomeroy & Li, 2000) |
| 9. Energy budget snowmelt (ebsm#1): | Calculates snowmelt for snowpack using energy balance of net radiation, sensible and latent heat, and advection from rainfall, and change in internal energy (Gray & Landine, 1988) |
| 10. Infiltration (frozenAyers): | Calculates snowmelt infiltration into frozen soils using Gray's snowmelt infiltration algorithm (Zhao & Gray, 1999) and rainfall infiltration into unfrozen soils on the basis of soil texture and ground cover (Ayers, 1959) |
| 11. Ground surface temperature (tsurface#3): | Calculates the ground surface temperature using air temperature and thermal conductivity and energy of snowpack during snow cover period on the basis of conduction approach (Luce & Tarboton, 2010) and using air temperature and net radiation for snow-free period on the basis of radiative–conductive–convective approach (Williams et al., 2015) |
| 12. Freeze and thaw soil layers (XG): | Freeze–thaw algorithm using a simplified solution of Stefan's heat flow equation (Changwei & Gough, 2013) for user defined number of soil layers; uses ground surface temperature as input |
| 13. Hydraulic conductivity (K_Estimate): | Estimates drainage factors on the basis of Darcy's law for unsaturated hydraulic conductivity using the Brooks and Corey relationship (Fang et al., 2013); provides the drainage factors for soil moisture balance module |
| 14. Soil moisture balance (SoilX): | Estimates soil moisture, groundwater flow, and interactions between groundwater and surface water (Fang et al., 2010; Leavesley, Lichty, Troutman, & Saindon, 1983); interacts with XG module to account for permafrost |
| 15. Muskingum distributed routing (Netroute_M_D): | Routes run-off between HRUs and to the sub-basin outlet using Muskingum method (Chow, 1964). The routing does not have to be linear; one HRU can contribute to multiple HRUs (Fang et al., 2010) |

Abbreviation: HRU, hydrological response unit.

elevation model, and derived from previous field research at Scotty Creek. The model was driven by a continuous hourly time series of incoming shortwave radiation, wind speed, relative humidity, air temperature, and precipitation (see Table 2 for instrumentation).

### 3.3.1 | CRHM input data and evaluation of model performance

Data collected over the period of August 2008 to August 2015 from two long-term micrometeorological tripods were compiled for CRHM modelling (see locations of tripods in Figure 1c). Given the rapidly changing landscape in this watershed, some permafrost loss surrounding the study channel fen did occur during this period (Chasmer & Hopkinson, 2016). However, given that localized permafrost loss around the perimeter of the study fen was reserved mainly to the northeastern side of the fen and did not result in the formation of any hydrological connections to surrounding wetland features, the landscape change during this model evaluation period is not considered here. Micrometeorological data from a tripod erected in an open bog was used to represent input data for modelled bog, channel fen, and lake area. Note that measured ET was only used for model evaluation and not used as model input. Separate input data were used for the peat plateau from a micrometeorological tripod installed below the canopy on a peat plateau. Input data equipment is described in Table 2. Data gaps less than 3 hr were filled using linear interpolation. Data gaps longer than 3 hr were filled using measurements from other

micrometeorological stations located on similar land cover types in the Scotty Creek basin.

As discharge measurements from the channel fen are not available for validation, four key hydrological variables were used to evaluate model performance: point snow depth, transect-based snow water equivalent (SWE), ET, and water table. Table 4 outlines availability of performance evaluation data according to HRU.

Simulated SWE was compared with measured SWE from snow surveys conducted annually from 2008 through to 2016 every 25 m along long-term established transects that intersected the bog and peat plateau tripod locations. Snow depth and density were measured at sampling points along the transects to determine SWE, and measured SWE for bog and peat plateau were calculated from averaged values for all points on the corresponding transects.

Evapotranspiration measurements for evaluation of model performance were was collected for both a bog ($ET_{bog}$) and for a mixed bog–peat plateau landscape ($ET_{land}$), which was derived from eddy covariance measurements as described by Helbig et al. (2016) and Warren et al. (2018). Briefly, a tripod located in a large open collapse-scar bog (Figure 1c) was instrumented with a sonic anemometer and an open-path infrared $CO_2/H_2O$ gas analyser (CSAT3A and EC150, Campbell Scientific, Logan, UT, USA) at 1.9 m above the moss surface in 2014 and was used to evaluate the performance of the "summer" period-modelled $ET_{bog}$ in 2014 and 2015 for the bog HRU. A micrometeorological tower (Figure 1c) was equipped with the same eddy covariance instrumentation above the forest canopy at 15 m above the moss surface in 2013. The eddy covariance flux footprint (see Helbig et al., 2016; Warren et al., 2018, for details) resulted in a landscape-scale $ET_{land}$ measurement of the combined bog and peat plateau ET (~50%–50%) during the summer in 2013, 2014, and 2015; no fen area is included in this measurement. Details regarding instrument set-up and processing of $ET_{bog}$ and $ET_{land}$ are described in Helbig et al. (2017). Flux footprint data quantifies the bog and peat plateau contributions (in per cent) to the half-hourly $ET_{land}$ measurements, which changes with wind direction, surface roughness, and atmospheric stability (see Helbig et al., 2016). Modelled bog and peat plateau ET were combined to create a modelled $ET_{land}$ using the same flux footprint contributions. Modelled $ET_{land}$ was then compared with the measured $ET_{land}$. For all years, modelled $ET_{bog}$ and $ET_{land}$ results were compared against measured hourly values for days with at least 75% measurement data coverage. Although model performance evaluations typically utilize cumulative weekly, monthly, or seasonal data (e.g., Fang et al., 2013), hourly ET data were used in this study as gaps in the data set limit representative cumulative ET over longer timescales.

**TABLE 4** Measured data used for performance evaluation

| Variable | HRU | Dates | Continuous? |
|---|---|---|---|
| Snow depth (cm) | Plateau | Aug 2008–Aug 2013 | Yes, SR50 (Campbell Scientific Canada, Distance Sensor) |
| | Bog | Aug 2008–Aug 2015 | |
| SWE (mm) | Plateau | Mar 2009–Mar 2014 | No, annual snow survey |
| | Bog | Mar 2009–Mar 2015 | |
| ET (mm $hr^{-1}$) | Landscape | Apr 2014–Dec 2015 | Seasonally, measurement details in Helbig et al. (2016) |
| | Bog | May 2013–Dec 2015 | |
| Water level (mm) | Bog | June 2009–Aug 2015 | Seasonally, water level recorder |

Abbreviation: HRU, hydrological response unit.

The water table was recorded in the bog where the micrometeorological tripod was located (Figure 1c, equipment described in Table 2). The sensor was installed annually in the early summer after snowmelt and after the surface of the bog had thawed and was removed before soil freezing in the fall. The CRHM model output is a depth of water that is stored in the soil column. This depth of water was used to estimate the depth of water table above or below the ground surface using the following assumptions: (a) There is a small amount of water that cannot be drained as it is part of the nonactive porosity equal to 0.18 volumetric soil water content (Zhang et al., 2010); (b) all water between the ground surface and the saturated water table is held at this minimum saturation level; (c) all pore space below the water table is saturated with water; and (d) the water table is above the ground when the modelled depression storage, $S_d$, is larger than 0.0 mm. The depth to water table is considered positive when below ground and negative when above ground.

Four statistics were used to evaluate model performance by comparing outputs with corresponding observations: mean error (*me*), per cent bias (*pbias*), root mean square error (*rmse*), and normalized root mean square error (*nrmse*), as well as the sample size (*n*, Table 5). Statistics were calculated using the "hydroGOF" R package (Zambrano-Bigiarini, 2014). Additionally, model outputs were evaluated using graphical goodness-of-fit measures, including $r^2$ values associated with the linear regression of paired values represented in one-to-one plots and Nash–Sutcliffe efficiencies (*nse*; Nash & Sutcliffe, 1970) for time series where applicable.

### 3.3.2 | Sensitivity analysis—Land cover transition model runs

After evaluating the model performance, a sensitivity analysis was conducted to assess the impact of incremental permafrost loss compared with the 2010 permafrost extent on channel fen surface and subsurface flows by varying the ratio of wetland to peat plateau area in the modelled sub-basin. When peat plateau area is lost in Scotty Creek, it is not possible to predict what type of wetland (bog or channel fen) will replace the lost forested area. To account for this uncertainty, four scenarios of increased wetland area were defined: (a) The simulated peat plateau-reduced area is replaced by expanded bog area

**TABLE 5** Summary of statistics used to evaluate performance of model

| Variable | HRU | *me* | *pbias* (%) | *rmse* | *nrmse* (%) | *n* |
|---|---|---|---|---|---|---|
| Snow depth (cm) | Plateau | −7.6 | −31.8 | 11.7 | 45.2 | 43,835 |
| | Bog | 3.9 | 20.3 | 10.1 | 47.9 | 54,693 |
| SWE (mm) | Plateau | 2.0 | 1.7 | 18.2 | 40.4 | 6 |
| | Bog | 30.8 | 23.5 | 37.1 | 154.9 | 7 |
| ET (mm $hr^{-1}$) | Landscape | 0.012 | 10.1 | 0.058 | 73.7 | 3,063 |
| | Bog | 0.067 | 47.9 | 0.089 | 89.2 | 1,671 |
| Water level (mm) | Bog | 21.3 | 71.4 | 50.2 | 75.4 | 16,060 |

Abbreviations: ET, evapotranspiration; HRU, hydrological response unit; SWE, snow water equivalent.

(Scenario "All Bog"); (b) the ratio of channel fen-to-bog area of the 2010 HRU delineation in the modelled sub-basin is maintained, with expanded wetland area added at a ratio of 1.6:1 fen to bog (Scenario "sub-basin"); (c) the ratio of fen-to-bog area of the greater Scotty Creek watershed is used to determine the ratio at which simulated lost peat plateau area is replaced, with expanded wetland area added at a ratio of 1.9:1 fen to bog (Scenario "Scotty"); and (d) all simulated peat plateau reduced area is replaced by expanded fen area (Scenario "All Fen"). All four scenarios were modelled for 10%, 25%, and 50% permafrost reductions compared with the 2010 permafrost extent. Given that all modelled landscape features are considered hydrologically connected to the channel fen and have the potential to contribute run-off when moisture levels are sufficiently high to satisfy depressional storage in each feature, this model does not simulate the transient response anticipated as individual bogs are "captured" by the drainage network. Rather, this model represents the condition once the anticipated diminishing return threshold has been reached (Haynes et al., 2018), wherein further permafrost loss does not establish hydrological connections between features and the period of transient wetland contributions has passed.

To examine the potential changes in the hydrological behaviour of the sub-basin with these scenarios, average annual run-off to precipitation ratios between 2009 and 2015 were calculated as the total discharge from the fen HRU divided by the precipitation as recorded by the weighing gauge after wind undercatch correction. To examine seasonal impacts, run-off ratios were also calculated for a "snowmelt" period, defined as the time from the first modelled SWE loss after maximum SWE to the last day for which snow cover was present in any HRU, and a "summer" period, defined as the time between the first day after all snow is melted and September 30 of every year.

## 4 | RESULTS AND DISCUSSION

### 4.1 | Field water balance

Field monitoring of the water balance components provides insight into the dominant processes governing the hydrology of the channel fen sub-basin. The highest rates of surface run-off occurred during the spring freshet due to the formation of an ice layer at the fen surface observed during field studies, limiting or inhibiting infiltration of snowmelt water (Figure 3b). Approximately 58% of annual surface run-off from the fen occurred during the "spring" period (Table 1 and Figure 3b), which accounted for more than 95% of total discharge during the same time period. The water table reached an average maximum elevation of +230 mm above the ground surface of the fen and dropped to within 50 mm by June 1, 2015 midway between the lakes. In contrast, an area directly next to First Lake remained ponded to a minimum depth of +120 mm above the fen surface during the entire study. During the "summer" period (Table 1), the water table remained consistently near the fen surface and responded quickly to rain events. $ET_{fen}$ exceeded precipitation inputs over this period with a total $ET_{fen}$/rainfall ratio of 1.2 for the "summer" of 2015 (Figure 3a, c). The surrounding land cover types (peat plateau, connected bog cascades, and the upstream lake) consistently contributed to the fen and maintained a sufficiently high water level to allow high rates of evapotranspiration during this period. As $ET_{fen}$ rates decreased in the "fall" (Table 1 and Figure 3a), the change in storage in the fen became positive. Subsurface discharge from the fen during the "fall" period accounted for 45% of total subsurface discharge that occurred over the whole water balance period, September 2, 2014, to August 26, 2015 (Figure 3d). Discharge during the "winter" was limited to the subsurface, as the surface of the fen remained frozen until after the spring freshet with a maximum measured refreezing depth of 240 mm. Subsurface discharge during the "winter" period accounted for 18% of total annual subsurface discharge. Discharge out of the fen was of similar magnitude to subsurface inputs, with an average positive change in storage of 3.0 mm $day^{-1}$ between December 18, 2014, and April 3, 2015. The mechanisms governing the hydrology of the channel fen are summarized in a conceptual model in Figure 4, which informed the module selection for the CRHM model.

### 4.2 | Numerical model

#### 4.2.1 | Performance evaluation

*Snow depth and SWE*

The model adequately captured the variation in hourly measured snow depth in the peat plateau and bog with high (>0.85) $r^2$ values (Figure 5a,b). Underestimation of peat plateau snow depth (*pbias* = −31.8%) and an overestimation bias for bog snow depth

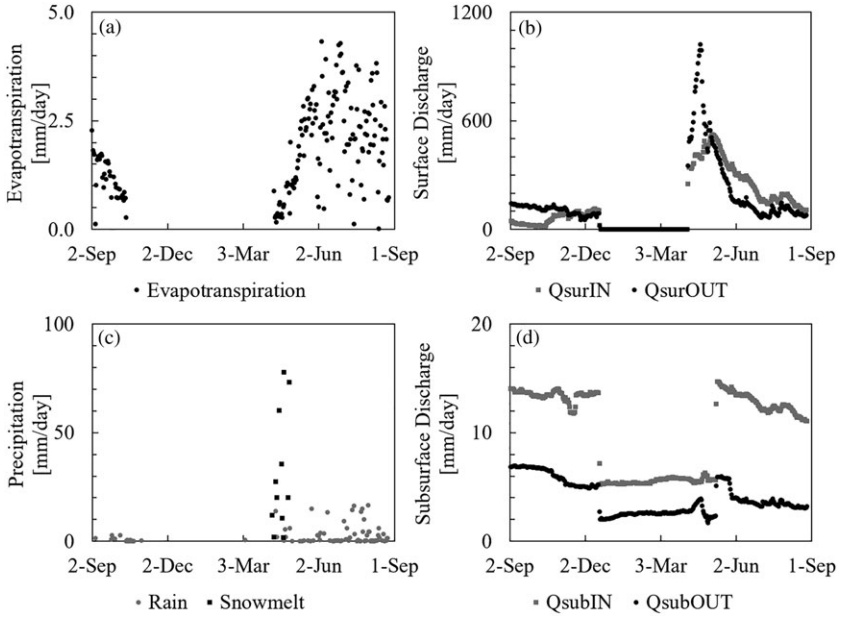


**FIGURE 3** Components of the water balance to determine the change in storage in the channel fen for the fall 2014 to fall 2015 time period including (a) evapotranspiration, (b) surface discharge in (QsurIN) and out (QsurOUT) of the channel fen, (c) precipitation inputs as either snowmelt or direct rainfall, and (d) subsurface discharge in (QsubIN) and out (QsubOUT) of the channel fen. Note different scales for each of the four panels

(*pbias* = 20.3%) was observed (Table 5 and Figure 5a,b). However, the high *nse* values (*nse* = 0.80 for plateau in Figure 5c, *nse* = 0.77 for bog in Figure 5d) and small *rmse* values (11.7 and 10.1 for plateau and bog, respectively; Table 5) for the simulation period suggest generally good model performance.

The disparity between the measured and modelled snow depth may in part be attributed to differences in scale and representation of spatial variability. The point snow depth measurements at the micrometeorological stations located on a single peat plateau and bog do not capture the natural spatial variability in snow distribution observed across landscape features. Therefore, modelled snow redistribution across the homogeneous HRUs may not perfectly align with the single-point snow depth measurements in each land cover type. However, given the differences in measured and modelled snow depth scales, these trends are in acceptable agreement.

The model adequately captured the variation in the measured SWE in the peat plateau and bog with $r^2$ values higher than 0.65 (Figure 6a,b). End of winter SWE was successfully captured for six winter seasons from 2009 to 2014 for the peat plateau (Figure 6c) with small positive bias (1.7%) as compared with the measured values (Table 5). The model tended to overestimate the end of season SWE for seven seasons from 2009 to 2015 for the bog (Figure 6d), with higher overestimation bias (23.5%) and larger difference compared with the measurements (Table 5). The average measured density during end-of-season snow surveys conducted in Scotty Creek on the bog land cover type between 2009 and 2015 is 170 kg/m$^3$, whereas

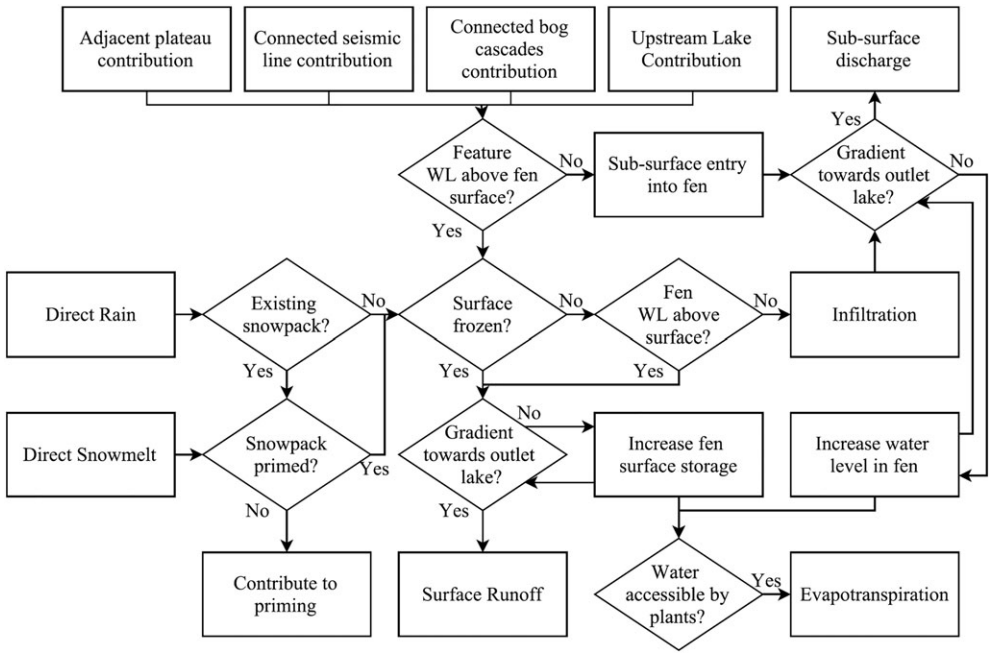


**FIGURE 4** Conceptual diagram of water movement through channel fens in wetland-dominated peat-rich basins in the discontinuous permafrost zone as determined through fieldwork conducted at the Scotty Creek Research Basin. Rectangles represent processes, whereas diamonds represent deterministic questions. Abbreviation: WL, water level. Note that bog cascades, seismic lines, and lakes may become hydrologically disconnected from a channel fen under sufficiently low water level conditions

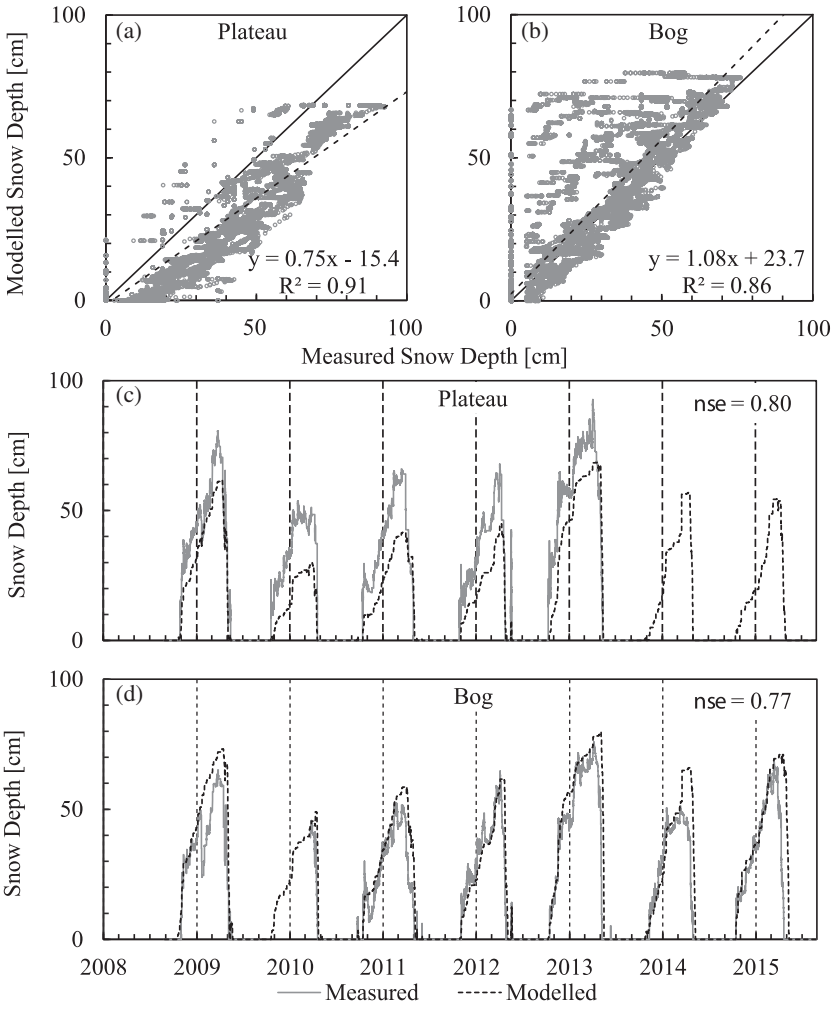


**FIGURE 5** One-to-one plots of (a) plateau and (b) bog snow depth; dashed black lines indicate linear regression. Time series data of (c) plateau and (d) bog snow depth. Vertical dashed lines indicate the end of the calendar year

the modelled snow density (obtained by dividing the modelled SWE by the modelled snow depth) for the same dates is 260 kg/m$^3$. The model appears to underestimate how much snow is sublimated or transported from the bog HRU, with an average difference between total snowfall and measured SWE between 2009 and 2015 of 36 mm and a modelled difference of 4 mm. In the peat plateau area, the model more accurately captured annual snow sublimation and transport processes, with a measured difference between snowfall and peat plateau SWE of 40 mm and a modelled difference of 42 mm during the same time period. Wind speeds measured in the bog (Figure 1c) are low and often below the model's threshold required to transport snow. Surface sublimation in the bog may have occurred, which is not effectively captured by the model. Alternatively, these disparities for the bog may suggest that the anemometer was inhibited by frost during the winter months resulting in the underestimation of blowing snow by the model.

The temporal resolution of measured snowpack SWE along the snow survey transects is limited to the end of the season prior to snowmelt. This approach therefore examines the properties of the snowpack that has been subjected to wind redistribution and metamorphism mechanisms, which influence snow depth, density, and SWE. Transect measurements spanned the different land cover types facilitating the incorporation of greater spatial variability to account for snow redistribution across these features. The homogeneity of each land cover HRU may not be fully representative of inherent natural variability and therefore contribute to the observed estimation biases when comparing the model results to the average SWE from end-of-season transect measurements. The limited temporal span of end-of-season snowpack SWE measurements, although typical in cold regions research, restricts the ability to validate modelled SWE over the course of the winter season.

*Evapotranspiration*

Modelled evapotranspiration was compared with measurements for each land cover type (i.e., bog, fen, and bog–plateau landscape). At the landscape scale, which incorporates only bog and peat plateau land covers, modelled $ET_{land}$ had a low overestimation bias (*pbias* = 10.1%) and relatively small difference compared with the measured $ET_{land}$ (Table 5), but modelled $ET_{land}$ was less variable (53% of measured $ET_{land}$ variation) and had a low $r^2$ value (Figure 7a). For the bog HRU, the model captured most of the variability of measured $ET_{bog}$ with a high $r^2$ value (Figure 7b), though the modelled $ET_{bog}$ showed an overestimation bias (*pbias* = 47.9%) and larger differences than for $ET_{land}$ (Table 5).

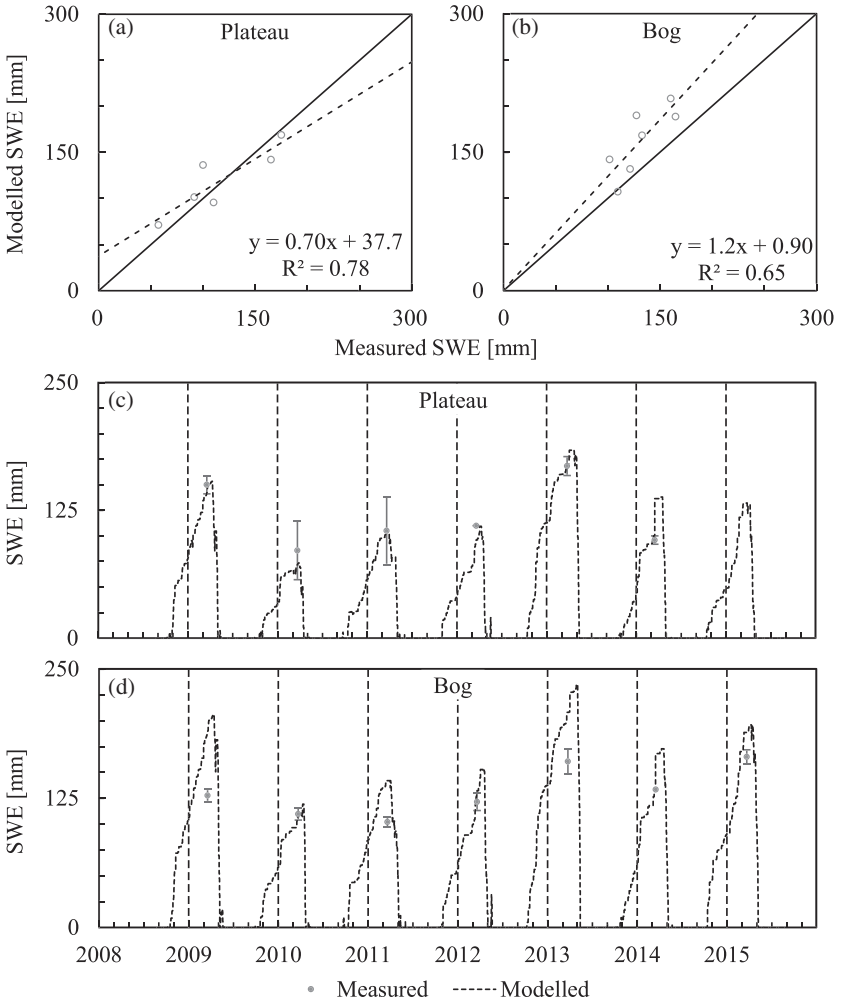


**FIGURE 6** One-to-one plots comparing modelled versus measured values for (a) plateau and (b) bog snow water equivalent; black dashed lines indicate the linear regression. Time series data of (c) plateau and (d) bog snow water equivalent; bars indicate standard error. Vertical dashed lines indicate the end of the calendar year. Abbreviation: SWE, snow water equivalent

Accurately modelling $ET_{bog}$ is important for estimating $ET_{land}$ as wetland ET can significantly exceed peat plateau ET due to higher moisture availability at the surface (Wright, Quinton, & Hayashi, 2008). Some of the ability to replicate $ET_{bog}$ versus $ET_{land}$ may be the result of the two different approaches used to model peat plateau ET (Penman–Monteith) and $ET_{bog}$ (Priestley–Taylor). Though the Priestley–Taylor method has been shown to accurately predict evaporation from peatlands with nonvascular coverage in Scotty Creek (Connon et al., 2015), peatlands with vascular plant cover are better represented by methods that account for atmospheric water vapour conditions in addition to net radiation such as the Penman–Monteith method (Lafleur & Roulet, 1992). The high availability of input data, including information on the surface conductance of black spruce trees (Zha et al., 2010) allowed for the application of the Penman–Monteith method to simulate peat plateau ET with a high coverage of vascular plants (Quinton et al., 2003). However, peat plateau tree density of Scotty Creek is sufficiently low (Chasmer, Quinton, Hopkinson, Petrone, & Whittington, 2011) to allow for significant contributions from the understory to peat plateau ET (Warren et al., 2018). As the conductance parameter used to calculate ET on the peat plateau area

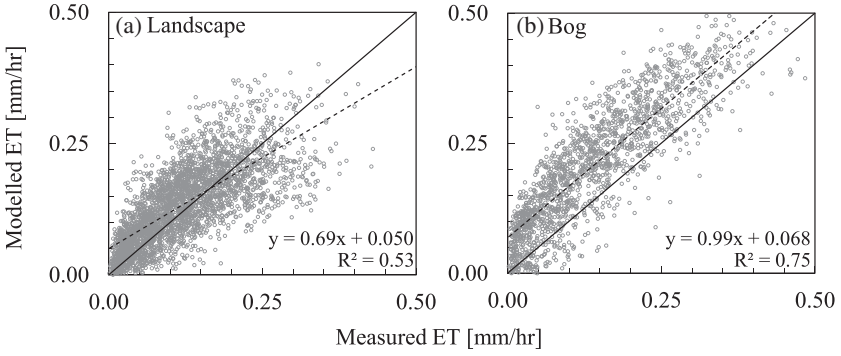


**FIGURE 7** One-to-one graphs comparing modelled versus measured values for (a) landscape and (b) bog evapotranspiration; dashed black lines indicate the linear regression. Abbreviation: ET, evapotranspiration

was based on studies on black spruce trees, it is possible that the model's inability to capture the variability in $ET_{land}$ may be due to the influence of understory conductance on the peat plateau features.

*Water table*

The model did not accurately simulate water table fluctuations in the summers of 2011 and 2014 but adequately captured the bog's measured water table fluctuations in other years (Figure 8c). On average, there was a 50-mm difference between the modelled and measured bog water table during the simulation period of 2008–2015 (Table 5). The collective overestimation bias for the modelled water table (*pbias* = 71.4%; Table 5) was driven by levels being simulated deeper than observed for the summers of 2011, 2012, 2013, and 2014. The model output, $S_d$, used in this performance evaluation for water table depth above the vegetated surface is a proxy. In the model, the output $S_d$ operates as a surface storage parameter and receives inputs not only from excess water in the underlying soil column but also receives precipitation inputs and run-off from upstream HRUs. This could explain some of the model's difficulty in simulating aboveground storage, for example, during the end of summer season of 2011 when the water table was above the ground surface and large late summer rain storms provided additional inputs.

## 4.3 | Sensitivity analysis

Although considerable uncertainty exists in some modelled water balance components in either the bog or peat plateau, the sensitivity analysis of the constructed model was carried out to examine the effects of loss of permafrost area on channel fen discharge. The disparities between modelled and observed data are likely a function of spatial and temporal scale. The parameterization of the available CRHM modules may not fully comprise the natural complexities of the mechanisms governing the hydrology of this dynamic landscape. The degree of model uncertainty should be considered when interpreting the following results. As such, only simulations of 50% permafrost loss are discussed in all sub-basin scenarios, when we expect permafrost thaw impacts to exceed model uncertainties.

For all four scenarios with varying relative proportions of fen and bog land area, and for all prescribed increments of permafrost loss, the modelled total annual discharge from the fen HRU decreased (Figure 9). On average, over the modelling period of 2009 to 2015, for every 10% of peat plateau area replaced with wetland area, there is an average decrease of 2.5% in total annual discharge from the fen. Scenario All Bog, in which the simulated reduction of permafrost-underlain peat plateau area is replaced entirely with an increase in bog area and no new fen area, results in the smallest decrease in fen discharge (Figure 9a). Scenario All Fen, where lost peat plateau permafrost area is replaced with fen area and no new bog area is modelled, results in the largest decrease in fen discharge (Figure 9d). The impacts of permafrost reduction on the annual discharge volume were variable from year to year depending on antecedent moisture conditions due to storage influences. The decrease in discharge from the fen HRU was greater in wet years, where discharge from the modelled sub-basin is larger than 200 mm $year^{-1}$. For instance, for the 50% permafrost reduction in Scenario sub-basin, annual cumulative discharge decreased by 53 mm (345 to 293 mm) in 2009 when water year precipitation was 598 mm but dropped by only 9 mm (168 to 149 mm) in 2013 when the water year precipitation of 348 mm was much less (Figure 9b).

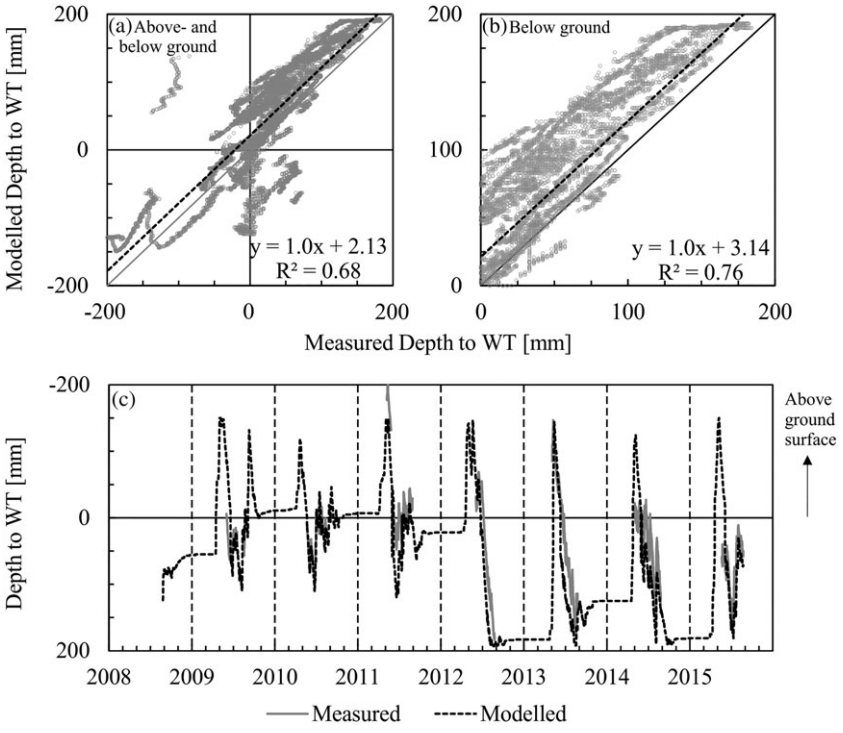


**FIGURE 8** (a) One-to-one graph comparing modelled versus measured water table values for above and below ground and (b) for below ground values only; dashed black lines represent the linear regression. (c) Time series of modelled and measured water table values. Vertical dashed lines indicate the end of the calendar year.
Abbreviation: WL, water level

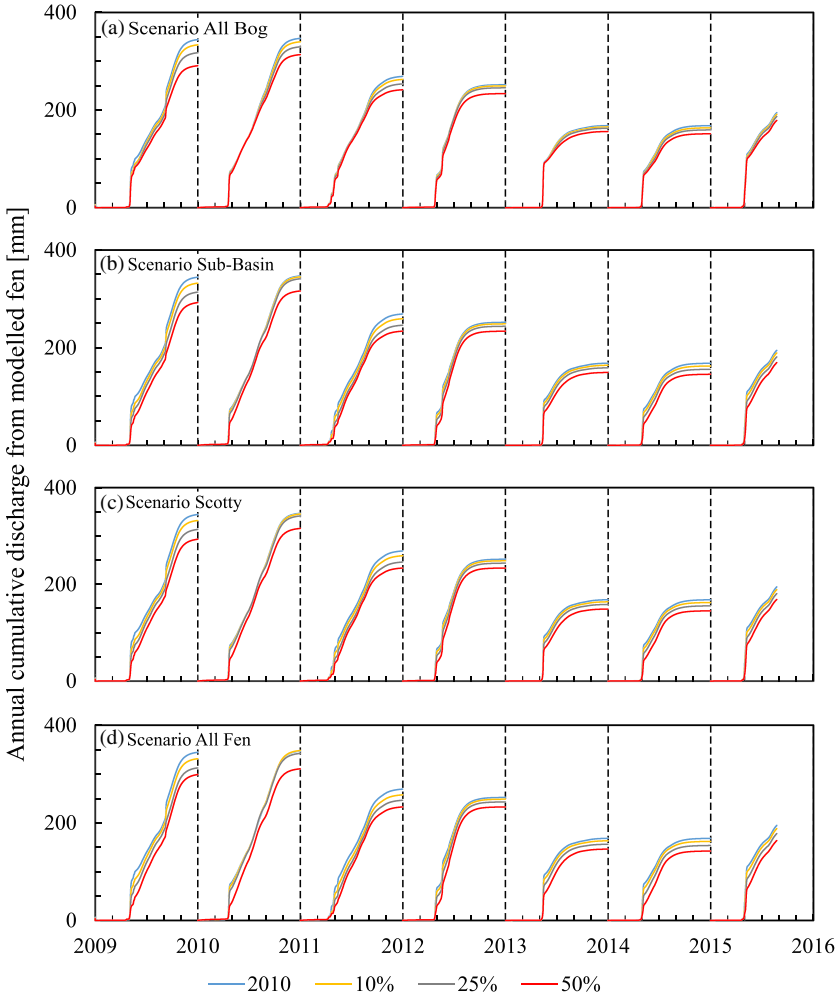


**FIGURE 9** Annual cumulative discharge from fen hydrological response unit for the modelled subarctic muskeg watershed for 10%, 25%, and 50% modelled permafrost loss compared with the 2010 permafrost extent for (a) Scenario All Bog, (b) Scenario sub-basin, (c) Scenario Scotty, and (d) Scenario All Fen. Vertical dashed lines indicate the end of the calendar year

Though the annual discharge from the fen HRU decreased in all scenarios, this does not hold true on a seasonal basis. Scenario sub-basin is used to illustrate this pattern (Figure 10c). During large late summer storms, identified as storms greater than 25 mm day$^{-1}$, and during spring snowmelt, the modelled hourly discharge from the fen HRU is up to 75% lower when compared with the 2010 permafrost extent modelled discharge depending on the percentage of permafrost loss. However, during low-flow periods just before the spring freshet begins and for extended periods in the summer, the hourly discharge from the fen HRU is greater than the 2010 modelled fen HRU discharge. To investigate this further, the total discharge from the fen HRU was separated into its three modelled layers: groundwater discharge (25–400 cm below surface), interflow (0–25 cm below surface), and surface run-off.

Scenario sub-basin is used to illustrate the change in discharge from the three modelled layers (Figure 11). The modelled increase in groundwater discharge (25–400 cm below the surface) compared with the 2010 permafrost extent was most pronounced during low-flow periods (e.g., August to December), and the annual cumulative difference was greatest in dry years (e.g., 2013 and 2014) with a total discharge of less than 200 mm year$^{-1}$ (Figure 11a). Groundwater reactivation due to thawing permafrost has been suggested as a major contribution to increased streamflow in permafrost-dominated regions (St. Jacques & Sauchyn, 2009). However, examination of winter flows, as a proxy to estimate baseflows, in the lower Liard Valley revealed that groundwater is not a primary driver of rising streamflows, accounting for less than 7% of total annual streamflow (Connon et al., 2014). The increased subsurface interflow (0- to 25-cm layer) is more prominent in wet years (e.g., 2009 and 2010, Figure 11b). As perched water tables lower with the loss of underlying permafrost bodies due to thaw, higher moisture availability is required to sustain flow in the near-surface soil. Even greater antecedent moisture levels are required to initiate surface flow paths, given the expanded soil moisture storage capacity in the permafrost-free peat profile. Surface discharge was most sensitive to permafrost reductions with greater magnitude decreases in flow as simulated permafrost area was lost (Figure 11c). With 50% permafrost loss, reductions in surface run-off ranged from 48% in a wet year (i.e., 2009) to 27% in a dry year (i.e., 2013). As permafrost bodies thaw and degrade, storage capacity in this land area increases (Quinton & Baltzer, 2013; Wright et al., 2009), thereby reducing the potential production of surface run-off. Coincidentally, the loss of permafrost barriers also facilitates enhanced interflow and groundwater exchange to a lesser extent as has been demonstrated in field studies across the discontinuous permafrost zone of the NWT in the lower Liard

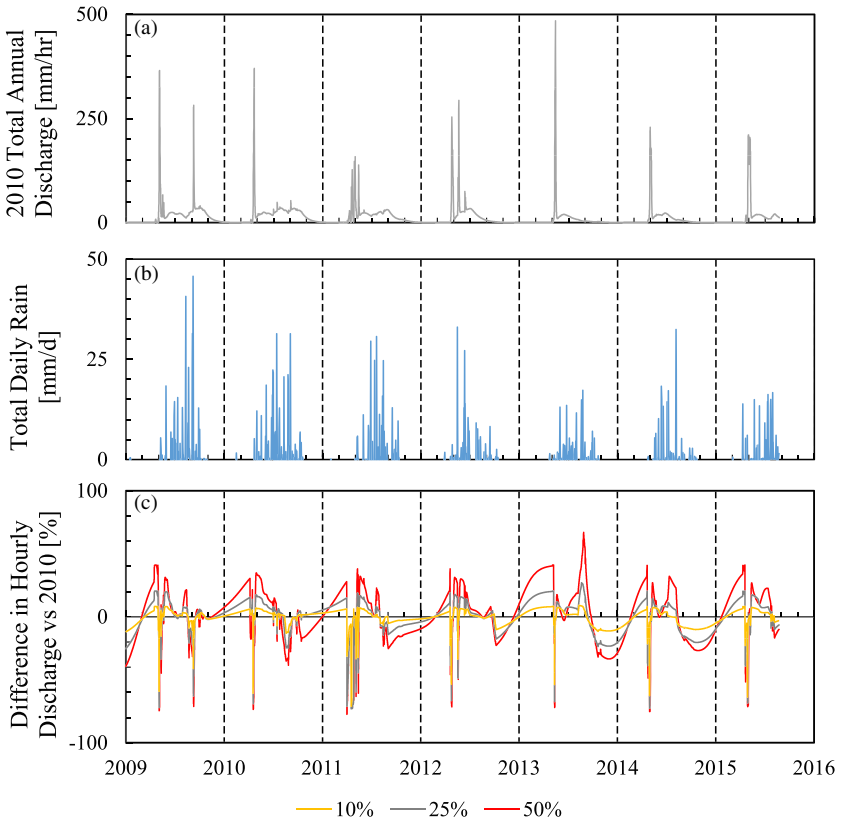


**FIGURE 10** (a) 2010 Total annual discharge out of the channel fen sub-basin with no simulated reduction in permafrost extent, (b) daily total rainfall in the fen hydrological response unit, and (c) per cent difference between the hourly discharge from the fen hydrological response unit comparing the Scenario sub-basin and the 2010 model run for simulated 10%, 25%, and 50% reduction in permafrost extent. Vertical dashed lines indicate the end of the calendar year

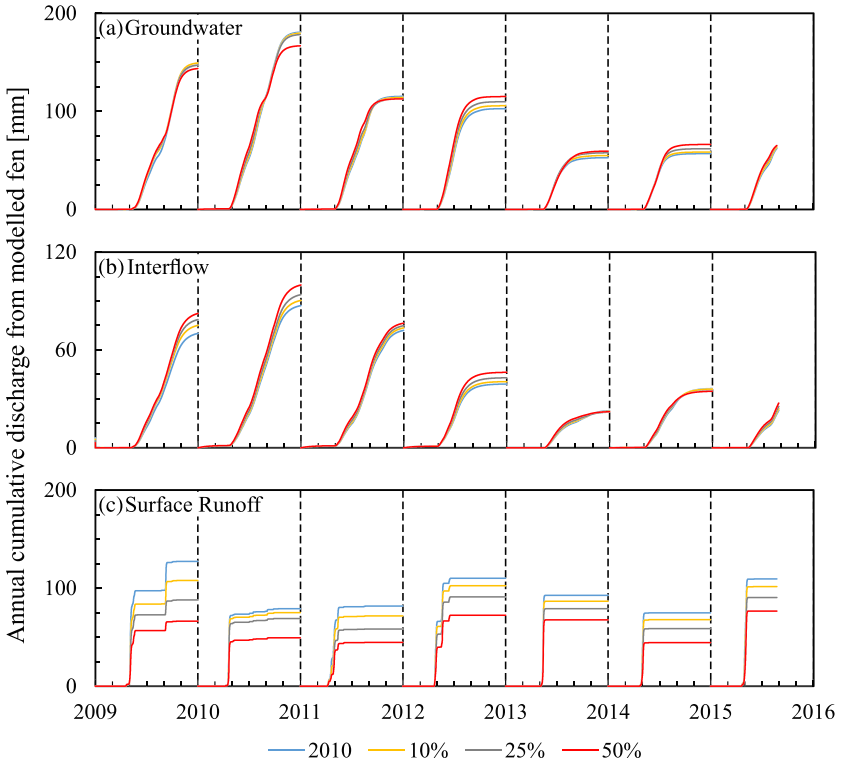


**FIGURE 11** Annual cumulative discharge from the fen hydrological response unit for the modelled subarctic muskeg watershed from the (a) groundwater zone (25–400 cm below fen surface), (b) interflow (0–25 cm below fen surface), and (c) surface run-off for Scenario sub-basin for the 2010 model run and for 10%, 25%, and 50% reduction in permafrost extent. Vertical dashed lines indicate the end of the calendar year. Note difference in *y*-axis scale for interflow plot

Valley (Connon et al., 2014). Though the discharge in both the 0- to 25-cm layer and the 25- to 400-cm layer of the channel fen increased with permafrost loss in the modelled sub-basin, reduction in surface run-off was not compensated for, resulting in an overall reduction in total annual discharge from the fen HRU in all scenarios and for all degrees of simulated permafrost loss.

The reduction in peak discharge and increased low flows is apparent when calculating run-off ratios based on simulated discharge

(Figure 10). The average annual run-off ratio for the 7-year period 2009–2015 was 0.54, assuming a constant areal permafrost extent equal to that in 2010. Reducing the permafrost coverage by 50% lowered the run-off ratio to 0.48, highlighting the modelled sub-basin's reduction in efficiency at exporting atmospheric inputs and enhanced storage. This change is most evident during the "snowmelt" period, where average snowmelt run-off ratios declined from 0.47 on the basis of the 2010 permafrost extent to 0.31 assuming a 50% reduction of permafrost extent. The "summer" period did not show this behaviour as average summer run-off ratios remained constant with 0.58 resulting from small increases in groundwater and interflow counteracting run-off reductions during small rainfall events in the low-flow periods.

Accurately modelling water table position and therefore potential available storage is important in understanding the hydrological response of the channel fen to precipitation events during the snow-free season. Collectively, these findings suggest that as permafrost continues to thaw annual discharge will decrease when all landscape features are capable of contributing to the drainage network, with the greatest decreases observed in surface flows. This is in contrast to current observed trends of increased discharge in the absence of increasing precipitation from discontinuous permafrost basins that are currently undergoing rapid dynamic changes due to permafrost thaw-induced landscape transition. Recent studies have highlighted increased hydrological connectivity during periods of sufficient moisture supply as a mechanism driving increases in basin discharge from Scotty Creek and elevated run-off ratios for the period of 1996–2012 (Connon et al., 2014), a trend that has continued through to 2017 (Haynes et al., 2018). A similar trend has been observed based on a combination of remote sensing data coupled with long-term hydroclimatic data, rather than field observations as in Connon et al. (2014) and Haynes et al. (2018), from this region (Chasmer & Hopkinson, 2016). However, the modelled sub-basin simulates sustained hydrological connections between the channel fen and the other HRUs including the adjacent bogs. Contributing area was held constant at its maximum extent and the land cover composition of the lost permafrost area was changed. When moisture levels are sufficiently high and depressional storage in each HRU is satisfied, all HRUs are capable of contributing to discharge, as there are no intervening permafrost barriers inhibiting flow. This state of widespread connectivity has been suggested to be an advanced stage of landscape change (Haynes et al., 2018), once the cascading process of "bog capture" has occurred throughout a drainage basin effectively incorporating all formerly isolated bog features into the drainage network (Connon et al., 2014). The process of connecting bogs to the drainage network through the loss of intervening permafrost barriers drains the water stored in the bog features and facilitates more direct flow paths contributing to run-off generation (Haynes et al., 2018). This establishment of a hydraulic connection results in a transient pulse of run-off as the water stored in the bog drains. Permanent increases to basin discharge when moisture levels are sufficiently high to trigger flow will likely result from landscape change due to the expansion in contributing area (Connon et al., 2014). However, the new level of discharge will likely be less than that currently observed as transient contributions from captured bogs decline with a fully connected basin (Haynes et al., 2018). The modelled channel fen in this study does not consider transient bog contributions but rather simulates the future scenario of a fully connected system with all HRUs having the potential to contribute hydrologically. The threshold response anticipated to occur as all landscape features develop the potential to hydrologically contribute to basin drainage (Chasmer & Hopkinson, 2016; Haynes et al., 2018) is not considered by this model simulation. Instead, this model examines the effects of further permafrost loss once the maximum level of hydrological connectivity has been achieved.

Seasonal variability in discharge is simulated to experience a dampening effect as a result of permafrost loss. Modelled discharge is higher during periods of low flow, whereas peak flows during late summer storms and the spring freshet are lower as permafrost thaws. This pattern of increased minimum discharge and decreased maximum discharge is a common pattern in basins undergoing permafrost degradation (e.g., Frampton, Painter, & Destouni, 2013). Some mechanisms that may explain these changes in wetland discharge include increases in basin ET and enhanced storage with land cover transition.

In the sensitivity analysis, the average annual total ET per unit area for any HRU is not changed, only relative HRU areas (Table 6). Across the land cover types of the basin headwaters, annual ET from bogs and channel fens is higher than from the peat plateaux. The sensitivity analysis shows that as the peat plateau area shrinks and wetland areas expand with permafrost degradation, the overall watershed ET flux increases, as also reported by Helbig et al. (2016). ET rates increase by on average 3.5% or the equivalent of 7.4 mm $km^{-2}$ annually for every 10% decrease in permafrost area compared with the 2010 extent. As ET is a major source of water loss from bogs (Connon et al., 2014) and at the basin scale has a magnitude of 65% to 70% of total incoming precipitation (Quinton & Hayashi, 2008), enhanced evapotranspiration could explain the lower WT and fewer instances of the water table rising above the ground surface to enable surface run-off.

Unlike peat plateaux, the bogs and fens in the sub-basin were parameterized to store water above the ground in topographic depressions. Therefore, when the modelled peat plateau area is reduced, the new land cover is one that contains depression storage. The depression storage in such areas functions as a hydrological buffer separating the run-off producing areas (i.e., peat plateaux) from the basin drainage network of channel fens (Shook & Pomeroy, 2011). Permafrost thaw-induced widening of this buffer therefore not only increases the flow length to reach the drainage network but also increases the amount of depression storage capacity that must be exceeded before run-off from the peat plateaux can reach the fen. As a result, the hydraulic response of channel fens will likely be increasingly attenuated with ongoing permafrost thaw. A widening wetland buffer and the loss of the perched water table on peat plateaux due to the degradation of the underlying permafrost body (Quinton & Baltzer, 2013; Wright et al., 2009) will also lower the elevation of the

**TABLE 6** Average annual total ET over the sub-basin

| Scenario | Lake | Bog | Fen | Plateau | sub-basin ET |
|---|---|---|---|---|---|
| | Percent of land cover (%) | | | | (mm km$^{-2}$) |
| Average ET (mm km$^{-2}$) | 156 | 384 | 388 | 92 | |
| 2010 Permafrost extent | 44 | 12 | 19 | 25 | 210 |
| Scenario sub-basin 10% | 44 | 13 | 20 | 23 | 218 |
| Scenario sub-basin 25% | 44 | 14 | 23 | 19 | 229 |
| Scenario sub-basin 50% | 44 | 16 | 27 | 13 | 247 |

Abbreviation: ET, evapotranspiration.

wetland water table because the hydrological input (e.g., snowmelt water) is distributed over a larger area and peat soil volume. As a result, greater hydrological input would be needed to overcome the depression storage capacity so that overland flow could occur.

## 5 | CONCLUSIONS

Reductions in permafrost extent decreased simulated total annual discharge from the channel fen due to increased surface storage capacity (Wright et al., 2009), reduced run-off efficiency, and increased basin-scale evapotranspiration (Helbig et al., 2016). Using a cold regions hydrological model, annual run-off was demonstrated to decrease with continued land cover change resulting from permafrost loss with a 2.5% reduction in total annual discharge for every 10% decrease in peat plateau area. Due to the limited temporal and spatial resolution of the data used for model validation and therefore the discrepancy in the model performance with such water balance components as snow depth and water level in the modelled landscape features as compared with observed data, considerable uncertainty may be factored into the model results. In general, as wetland area increases the peak discharge during high-flow events such as spring snowmelt and large late-summer storms decreases. In contrast, during low-flow periods conversion of peat plateau area to wetlands resulted in enhanced discharge. The routing of water through this landscape will likely also be influenced by permafrost loss with increases observed in total annual groundwater and interflow fluxes. As this model considers all basin features as hydrologically connected to the drainage network, these results may be indicative of the trajectory of landscape change in this region with all previously isolated wetland features undergoing "bog capture" as permafrost barriers degrade (Connon et al., 2014). Observed short-term increases in basin run-off with draining of wetlands and expansion of contributing area (Haynes et al., 2018) are expected to reach a point of diminishing return of further landscape connection. Increased drainage, catalysed as all features of these transitioning landscapes become hydrologically connected with the potential to contribute to basin run-off in periods of sufficient moisture supply (Haynes et al., 2018), is anticipated to promote afforestation with the re-establishment of dense tree canopies in these environments over time (Carpino, Berg, Quinton, & Adams, 2018). Some growth of trees has been observed in wetland environments in the Scotty Creek watershed as the hydrology of the landscape changes (Chasmer & Hopkinson, 2016). The trajectory of landscape change will likely result in elevated run-off from the discontinuous permafrost landscape as compared with prior to considerable permafrost thaw but lower than current conditions with dynamic change resulting in transient drainage of wetland features, which contribute stored water to drainage as they form connections to the drainage network (Haynes et al., 2018). The fully connected landscape simulated in this modelling exercise is likely to result in reduced basin outflow. Further research into the effects of afforestation of wetland environments with enhanced basin drainage would strengthen the understanding of the hydrological impacts of permafrost thaw in the discontinuous permafrost zone and would benefit modelling efforts of the trajectory of thaw-induced landscape change.

## ACKNOWLEDGEMENTS

We would like to thank the Natural Sciences and Engineering Research Council of Canada (NSERC), the NSERC Changing Cold Regions Network (CCRN),the NSERC Climate Change and Atmospheric Research Initiative, and the Northern Scientific Training Program for their support through funding for the Scotty Creek research station and this research. We would also like to thank the Government of the Northwest Territories (GNWT) for their support through the Laurier-GNWT Partnership Agreement. Thank you to Dr Kevin Shook of the Centre for Hydrology for support on CRHMr package used in the R statistical computing environment. Thank you to Karoline Wischnewski, Élise Devoie, Jared Simpson, Élyse Mathieu, and Ryan Connon for field assistance and advice. We would also like to acknowledge the generous support from the Liidlii Kue First Nation, the Dehcho First Nations, and the town of Fort Simpson. This manuscript is adapted from the M.Sc. thesis of L. Stone, Wilfrid Laurier University (Stone, 2018).

## DATA AVAILABILITY STATEMENT

The data that support the findings of this study are available from the corresponding author upon reasonable request.

## ORCID

*Kristine M. Haynes* https://orcid.org/0000-0002-9529-4640

## REFERENCES


Ayers, H. D. (1959). Influence of soil profile and vegetation characteristics on net rainfall supply to runoff. In Proceedings of Hydrology Symposium (Vol. *1*, pp. 198-205).

Aylsworth, J. M., Burgess, M. M., Desrochers, D. T., Duk-Rodkin, A., Robertson, T., & Traynor, J. A. (2000). Surficial geology, subsurface materials, and thaw sensitivity of sediments. *Geological Survey of Canada Bulletin*, *547*, 41–48.

Aylsworth, J. M., & Kettles, I. M. (2000). Distribution of fen and bog in the Mackenzie Valley, 60°N–60°N. *Geological Survey of Canada Bulletin*, *547*, 49–55.

Baltzer, J. L., Veness, T., Chasmer, L. E., Sniderhan, A. E., & Quinton, W. L. (2014). Forests on thawing permafrost: Fragmentation, edge effects, and net forest loss. *Global Change Biology*, *20*(3), 824–834. https://doi.org/10.1111/gcb.12349

Brunt, D. (1932). Notes on radiation in the atmosphere. *Quarterly Journal of the Royal Meteorological Society*, *58*(247), 389–420.

Burgess, M. M., & Smith, S. L. (2000). Shallow ground temperatures. The physical environment of the Mackenzie Valley, Northwest Territories: A base line for the assessment of environmental change. *Geological Survey of Canada Bulletin*, *547*, 89–103.

Camill, P. (2005). Permafrost thaw accelerates in boreal peatlands during late-20th century climate warming. *Climatic Change*, *68*(1), 135–152. https://doi.org/10.1007/s10584-005-4785-y

Carpino, O., Berg, A., Quinton, W., & Adams, J. (2018). Climate change and permafrost thaw-induced boreal forest loss in northwestern Canada. *Environmental Research Letters*, *13*, 084018. https://doi.org/10.1088/1748-9326/aad74e

Changwei, X., & Gough, W. A. (2013). A simple thaw-freeze algorithm for a multi-layered soil using the Stefan equation. *Permafrost and Periglacial Processes*, *24*(3), 252–260. https://doi.org/10.1002/ppp.1770

Chasmer, L., & Hopkinson, C. (2016). Threshold loss of discontinuous permafrost and landscape evolution. *Global Change Biology*, *23*, 2672–2686.

Chasmer, L., Hopkinson, C., & Quinton, W. (2010). Quantifying errors in discontinuous permafrost plateau change from optical data, Northwest Territories, Canada: 1947–2008. *Canadian Journal of Remote Sensing*, *36*(S2), S211–S223. https://doi.org/10.5589/m10-058

Chasmer, L., Hopkinson, C., Veness, T., Quinton, W., & Baltzer, J. (2014). A decision-tree classification for low-lying complex land cover types within the zone of discontinuous permafrost. *Remote Sensing of Environment*, *143*, 73–84. https://doi.org/10.1016/j.rse.2013.12.016

Chasmer, L., Quinton, W., Hopkinson, C., Petrone, R., & Whittington, P. (2011). Vegetation canopy and radiation controls on permafrost plateau evolution within the discontinuous permafrost zone, Northwest Territories, Canada. *Permafrost and Periglacial Processes*, *22*(3), 199–213.

Chow, V. T. (1964). *Handbook of applied hydrology*. New York: McGraw-Hill, Inc.

Connon, R. F., Quinton, W. L., Craig, J. R., Hanisch, J., & Sonnentag, O. (2015). The hydrology of interconnected bog complexes in discontinuous permafrost terrains. *Hydrological Processes*, *29*(18), 3831–3847. https://doi.org/10.1002/hyp.10604

Connon, R. F., Quinton, W. L., Craig, J. R., & Hayashi, M. (2014). Changing hydrologic connectivity due to permafrost thaw in the lower Liard River valley, NWT, Canada. *Hydrological Processes*, *28*(14), 4163–4178. https://doi.org/10.1002/hyp.10206

Dimitrov, D. D., Bhatti, J. S., & Grant, R. F. (2014). The transition zones (ecotone) between boreal forests and peatlands: Ecological controls on ecosystem productivity along a transition zone between upland black spruce forest and a poor forested fen in central Saskatchewan. *Ecological Modelling*, *291*, 96–108. https://doi.org/10.1016/j.ecolmodel.2014.07.020

Ellis, C. R., Pomeroy, J. W., Brown, T., & MacDonald, J. (2010). Simulation of snow accumulation and melt in needleleaf forest environments. *Hydrology and Earth System Sciences*, *14*(6), 925–940. https://doi.org/10.5194/hess-14-925-2010

Environment and Climate Change Canada (2017). Canadian climate normals 1981–2010 station data (Fort Simpson A) [Data file]. Retrieved from http://climate.weather.gc.ca/climate_normals/

Fan, S. M., Wofsy, S. C., Bakwin, P. S., Jacob, D. J., & Fitzjarrald, D. R. (1990). Atmosphere-biosphere exchange of $CO_2$ and $O_3$ in the Central Amazon Forest. *Journal of Geophysical Research-Atmospheres*, *95*, 16851–16864. https://doi.org/10.1029/JD095iD10p16851

Fang, X., & Pomeroy, J. W. (2016). Impact of antecedent conditions on simulations of a flood in a mountain headwater basin. *Hydrological Processes*, *30*(16), 2754–2772. https://doi.org/10.1002/hyp.10910

Fang, X., Pomeroy, J. W., Ellis, C. R., MacDonald, M. K., DeBeer, C. M., & Brown, T. (2013). Multi-variable evaluation of hydrological model predictions for a headwater basin in the Canadian Rocky Mountains. *Hydrology and Earth System Sciences*, *17*(4), 1635–1659. https://doi.org/10.5194/hess-17-1635-2013

Fang, X., Pomeroy, J. W., Westbrook, C. J., Guo, X., Minke, A. G., & Brown, T. (2010). Prediction of snowmelt derived streamflow in a wetland dominated prairie basin. *Hydrology and Earth System Sciences*, *14*(6), 991–1006. https://doi.org/10.5194/hess-14-991-2010

Frampton, A., Painter, S. L., & Destouni, G. (2013). Permafrost degradation and subsurface-flow changes caused by surface warming trends. *Hydrogeology Journal*, *21*(1), 271–280. https://doi.org/10.1007/s10040-012-0938-z

Frey, K. E., & McClelland, J. W. (2009). Impacts of permafrost degradation on arctic river biogeochemistry. *Hydrological Processes*, *23*(1), 169–182. https://doi.org/10.1002/hyp.7196

Fritz, C., Campbell, D. I., & Schipper, L. A. (2008). Oscillating peat surface levels in a restiad peatland, New Zealand—Magnitude and spatiotemporal variability. *Hydrological Processes*, *22*(17), 3264–3274. https://doi.org/10.1002/hyp.6912

Garnier, B. J., & Ohmura, A. (1970). The evaluation of surface variations in solar radiation income. *Solar Energy*, *13*(1), 21–34. https://doi.org/10.1016/0038-092X(70)90004-6

Gordon, J., Quinton, W., Branfireun, B. A., & Olefeldt, D. (2016). Mercury and methylmercury biogeochemistry in a thawing permafrost wetland complex, Northwest Territories, Canada. *Hydrological Processes*, *30*(20), 3627–3638. https://doi.org/10.1002/hyp.10911

Granger, R. J., & Gray, D. M. (1990). A net radiation model for calculating daily snowmelt in open environments. *Hydrology Research*, *21*(4–5), 217–234. https://doi.org/10.2166/nh.1990.0017

Gray, D. M., & Landine, P. G. (1988). An energy-budget snowmelt model for the Canadian Prairies. *Canadian Journal of Earth Sciences*, *25*(8), 1292–1303. https://doi.org/10.1139/e88-124

Harder, P., & Pomeroy, J. W. (2014). Hydrological model uncertainty due to precipitation phase partitioning methods. *Hydrological Processes*, *28*, 4311–4327. https://doi.org/10.1002/hyp.10214

Hayashi, M., & Quinton, W. L. (2005) [Salt-tracer test for saturated hydraulic conductivity in channel fen, Scotty Creek]. Unpublished raw data.

Hayashi, M., Quinton, W. L., Pietroniro, A., & Gibson, J. J. (2004). Hydrologic functions of wetlands in a discontinuous permafrost basin indicated by isotopic and chemical signatures. *Journal of Hydrology*, *296*(1), 81–97. https://doi.org/10.1016/j.jhydrol.2004.03.020

Haynes, K. M., Connon, R. F., & Quinton, W. L. (2018). Permafrost thaw induced drying of wetlands at Scotty Creek, NWT, Canada. *Environmental Research Letters*, *13*, 114001. https://doi.org/10.1088/1748-9326/aae46c

Helbig, M., Chasmer, L., Kljun, N., Quinton, W., Treat, C., & Sonnentag, O. (2017). The positive net radiative greenhouse has forcing of increasing methane emissions from a thawing boreal forest-wetland landscape.

*Global Change Biology*, *23*(6), 2413–2427. https://doi.org/10.1111/gcb.13520

Helbig, M., Chasmer, L. E., Desai, A. R., Klun, N., Quinton, W. L., & Sonnentag, O. (2017). Direct and indirect climate change effects on carbon dioxide fluxes in a thawing boreal forest-wetland landscape. *Global Change Biology*, *23*, 3231–3248. https://doi.org/10.1111/gcb.13638

Helbig, M., Wischnewski, K., Kljun, N., Chasmer, L. E., Quinton, W. L., Detto, M., & Sonnentag, O. (2016). Regional atmospheric cooling and wetting effect of permafrost thaw-induced boreal forest loss. *Global Change Biology*, *22*(12), 4048–4066. https://doi.org/10.1111/gcb.13348

Horst, T. W. (1997). A simple formula for attenuation of eddy fluxes measured with first order response scalar sensors. *Boundary-Layer Meteorology*, *94*, 517–520.

IPCC (2014). Impacts, adaptation, and vulnerability. Part B: Regional aspects. In *Contribution of working group II to the Fifth assessment report of the intergovernmental panel on climate change*. Cambridge, United Kingdom and New York: Cambridge Univesity Press.

Jorgenson, M. T., Racine, C. H., Walters, J. C., & Osterkamp, T. E. (2001). Permafrost degradation and ecological changes associated with a warming climate in central Alaska. *Climatic Change*, *48*(4), 551–579. https://doi.org/10.1023/A:1005667424292

Kozlowski, T. T. (Ed.) (1984). *Flooding and plant growth* (p. 356). New York: Academic Press.

Krogh, S. A., & Pomeroy, J. W. (2018). Recent changes to the hydrological cycle of an Arctic basin at the tundra-taiga transition. *Hydrology and Earth System Sciences Discussions*, *22*(7), 3993–4014. https://doi.org/10.5194/hess-2018-115

Kwong, Y. J., & Gan, T. Y. (1994). Northward migration of permafrost along the Mackenzie Highway and climatic warming. *Climatic Change*, *26*(4), 399–419. https://doi.org/10.1007/BF01094404

Lafleur, P. M., & Roulet, N. T. (1992). A comparison of evaporation rates from two fens of the Hudson Bay Lowland. *Aquatic Botany*, *44*(1), 59–69. https://doi.org/10.1016/0304-3770(92)90081-S

Leavesley, G. H., Lichty, R. W., Troutman, B. M., & Saindon, L. G. (1983). *Precipitation-runoff modelling system: User's manual. Report 83–4238* (p. 207). Washington DC, US: US Geological Survey Water Resources Investigations.

López-Moreno, J. I., Pomeroy, J. W., Revuelto, J., & Vicente-Serrano, S. M. (2012). Response of snow processes to climate change: Spatial variability in a small basin in the Spanish Pyrenees. *Hydrological Processes*, *27*(18), 2637–2650.

Luce, C. H., & Tarboton, D. G. (2010). Evaluation of alternative formulae for calculation of surface temperature in snowmelt models using frequency analysis of temperature observations. *Hydrology and Earth System Sciences*, *14*(3), 535–543. https://doi.org/10.5194/hess-14-535-2010

Marsh, P., Russell, M., Pohl, S., Haywood, H., & Onclin, C. (2009). Changes in thaw lake drainage in the Western Canadian Arctic from 1950 to 2000. *Hydrological Processes*, *23*(1), 145–158. https://doi.org/10.1002/hyp.7179

Massman, W. J. (2000). A simple method for estimating frequency response corrections for eddy covariance systems. *Agricultural and Forest Meteorology*, *104*, 185–198. https://doi.org/10.1016/S0168-1923(00)00164-7

Mauder, M., & Foken, T. (2006). Impact of post-field data processing on eddy covariance flux estimates and energy balance closure. *Meteorologische Zeitschrift*, *15*(6), 597–609. https://doi.org/10.1127/0941-2948/2006/0167

McClymont, A. F., Hayashi, M., Bentley, L. R., & Christensen, B. S. (2013). Geophysical imaging and thermal modeling of subsurface morphology and thaw evolution of discontinuous permafrost. *Journal of Geophysical Research*, *118*, 1826–1837. https://doi.org/10.1002/jgrf.20114.2013

Monteith, J. L. (1965). Evaporation and environment. In state and movement of water in living organisms. 19th Symposium of the Society for Experimental Biology. Cambridge University Press: Cambridge; 205–234.

Nash, J. E., & Sutcliffe, J. V. (1970). River flow forecasting through conceptual models, Part I—A discussion of principles. *Journal of Hydrology*, *10*, 282–290. https://doi.org/10.1016/0022-1694(70)90255-6

O'Donnell, J. A., Jorgenson, M. T., Harden, J. W., McGuire, A. D., Kanevskiy, M. Z., & Wickland, K. P. (2012). The effects of permafrost thaw on soil hydrologic, thermal, and carbon dynamics in an Alaskan peatland. *Ecosystems*, *15*(2), 213–229. https://doi.org/10.1007/s10021-011-9504-0

Pan, X., Yang, D., Li, Y., Barr, A., Helgason, W., Hayashi, M., … Janowicz, R. J. (2016). Bias corrections of precipitation measurements across experimental sites in different ecoclimatic regions of western Canada. *The Cryosphere*, *10*(5), 2347–2360. https://doi.org/10.5194/tc-10-2347-2016

Patankar, R., Quinton, W. L., Hayashi, M., & Baltzer, J. L. (2015). Sap flow responses to seasonal thaw and permafrost degradation in a subarctic boreal peatland. *Trees*, *29*(1), 129–142. https://doi.org/10.1007/s00468-014-1097-8

Pomeroy, J. W., Gray, D. M., Brown, T., Hedstrom, N. R., Quinton, W. L., Granger, R. J., & Carey, S. K. (2007). The cold regions hydrological model: A platform for basing process representation and model structure on physical evidence. *Hydrological Processes*, *21*(19), 2650–2667. https://doi.org/10.1002/hyp.6787

Pomeroy, J. W., & Li, L. (2000). Prairie and arctic areal snow cover mass balance using a blowing snow model. *Journal of Geophysical Research-Atmospheres*, *105*(D21), 26619–26634. https://doi.org/10.1029/2000JD900149

Priestley, C. H. B., & Taylor, R. J. (1972). On the assessment of surface heat flux and evaporation using large-scale parameters. *Monthly Weather Review*, *100*(2), 81–92. https://doi.org/10.1175/1520-0493(1972)100<0081:OTAOSH>2.3.CO;2

Quinton, W. L., & Baltzer, J. L. (2013). The active-layer hydrology of a peat plateau with thawing permafrost (Scotty Creek, Canada). *Hydrogeology Journal*, *21*(1), 201–220. https://doi.org/10.1007/s10040-012-0935-2

Quinton, W. L., & Hayashi, M. (2008). Recent advances toward physically-based runoff modeling of the wetland-dominated Central Mackenzie River basin. In *Cold region atmospheric and hydrologic studies. The Mackenzie GEWEX experience* (pp. 257–279). Berlin Heidelberg: Springer. https://doi.org/10.1007/978-3-540-75136-6_14

Quinton, W. L., Hayashi, M., & Chasmer, L. E. (2009). Peatland hydrology of discontinuous permafrost in the Northwest Territories: Overview and synthesis. *Canadian Water Resources Journal*, *34*(4), 311–328. https://doi.org/10.4296/cwrj3404311

Quinton, W. L., Hayashi, M., & Chasmer, L. E. (2011). Permafrost-thaw-induced land-cover change in the Canadian subarctic: Implications for water resources. *Hydrological Processes*, *25*(1), 152–158. https://doi.org/10.1002/hyp.7894

Quinton, W. L., Hayashi, M., & Pietroniro, A. (2003). Connectivity and storage functions of channel fens and flat bogs in northern basins. *Hydrological Processes*, *17*(18), 3665–3684. https://doi.org/10.1002/hyp.1369

R Core Team (2017). R: A language and environment for statistical computing. R Foundation for statistical computing, Vienna, Austria. URL https://www.R-project.org/.

Shook, K. (2016). CRHMr: Pre- and post-processing for CRHM. R Package Version 2.4.10. https://github.com/CentreForHydrology/CRHMr

Shook, K. R., & Pomeroy, J. W. (2011). Memory effects of depressional storage in Northern Prairie hydrology. *Hydrological Processes*, *25*, 3890–3898. https://doi.org/10.1002/hyp.8381

Sicart, J. E., Pomeroy, J. W., Essery, R. L. H., & Bewley, D. (2006). Incoming longwave radiation to melting snow: Observations, sensitivity and

estimation in northern environments. *Hydrological Processes*, *20*(17), 3697–3708. https://doi.org/10.1002/hyp.6383

Sjöberg, Y., Coon, E., Sannel, A. B. K., Pannetier, R., Harp, D., Frampton, A., … Lyon, S. W. (2016). Thermal effects of groundwater flow through subarctic fens: A case study based on field observations and numerical modeling. *Water Resources Research*, *52*(3), 1591–1606. https://doi.org/10.1002/2015WR017571

Smith, C. D. (2007). Correcting the wind bias in snowfall measurements made with a Geonor T-200B precipitation gauge and alter wind shield. In 87th American Meteorological Society annual meeting, San Antonio, TX.

Smith, S. L., Burgess, M. M., Riseborough, D., & Nixon, F. M. (2005). Recent trends from Canadian permafrost thermal monitoring network sites. *Permafrost and Periglacial Processes*, *16*(1), 19–30. https://doi.org/10.1002/ppp.511

St. Jacques, J. M., & Sauchyn, D. J. (2009). Increasing winter baseflow and mean annual streamflow from possible permafrost thawing in the Northwest Territories, Canada. *Geophysical Research Letters*, *36*(1), L01401. https://doi.org/10.1029/2008GL035822

Stone, L. (2018). The role of channel fens in permafrost degradation induced changes in peatland discharge at Scotty Creek, NT. Wilfrid Laurier University Theses and Dissertations (Comprehensive). 2021. https://scholars.wlu.ca/etd/2021

Taylor, A. E., Wang, K., Smith, S. L., Burgess, M. M., & Judge, A. S. (2006). Canadian Arctic Permafrost Observatories: Detecting contemporary climate change through inversion of subsurface temperature time series. *Journal of Geophysical Research - Solid Earth*, *111*(B2). https://doi.org/10.1029/2004JB003208

Verseghy, D. L. (1991). CLASS—A Canadian land surface scheme for GCMs. I. Soil Model. *International Journal of Climatology*, *11*(2), 111–133.

Vickers, D., & Mahrt, L. (1997). Quality control and flux sampling problems for tower and aircraft data. *Journal of Atmospheric and Oceanic Technology*, *14*, 512–526. https://doi.org/10.1175/1520-0426(1997)014<0512:QCAFSP>2.0.CO;2

Warren, R. K., Pappas, C., Helbig, M., Chasmer, L. E., Berg, A. A., Baltzer, J. L., … Sonnentag, O. (2018). Minor contribution of overstorey transpiration to landscape evapotranspiration in boreal permafrost peatlands. *Ecohydrology*, *11*. https://doi.org/10.1002/eco.1975

Webb, E. K., Pearman, G. I., & Leuning, R. (1980). Correction of flux measurements for density effects due to heat and water vapour transfer. *Quarterly Journal of the Royal Meteorological Society*, *106*, 85–100. https://doi.org/10.1002/qj.49710644707

Williams, T. J., Pomeroy, J. W., Janowicz, J. R., Carey, S. K., Rasouli, K., & Quinton, W. L. (2015). A radiative–conductive–convective approach to calculate thaw season ground surface temperatures for modelling frost table dynamics. *Hydrological Processes*, *29*(18), 3954–3965. https://doi.org/10.1002/hyp.10573

Wright, N., Hayashi, M., & Quinton, W. L. (2009). Spatial and temporal variations in active layer thawing and their implication on runoff generation in peat-covered permafrost terrain. *Water Resources Research*, *45*, W05414.

Wright, N., Quinton, W. L., & Hayashi, M. (2008). Hillslope runoff from an ice-cored peat plateau in a discontinuous permafrost basin, Northwest Territories, Canada. *Hydrological Processes*, *22*(15), 2816–2828. https://doi.org/10.1002/hyp.7005

Zambrano-Bigiarini, M. (2014). hydroGOF: Goodness-of-fit functions for comparison of simulated and observed hydrological times series. R Package Version 0.3–8. https://CRAN.R-project.org/package=hydroGOF

Zha, T., Barr, A. G., van der Kamp, G., Black, T. A., McCaughey, J. H., & Flanagan, L. B. (2010). Interannual variation of evapotranspiration from forest and grassland ecosystems in western Canada in relation to drought. *Agricultural and Forest Meteorology*, *150*(11), 1476–1484. https://doi.org/10.1016/j.agrformet.2010.08.003

Zhang, Y., Carey, S. K., Quinton, W. L., Janowicz, J. R., Pomeroy, J. W., & Flerchinger, G. N. (2010). Comparison of algorithms and parameterisations for infiltration into organic-covered permafrost soils. *Hydrology and Earth System Sciences*, *14*(5), 729–750. https://doi.org/10.5194/hess-14-729-2010

Zhao, L., & Gray, D. M. (1999). Estimating snowmelt infiltration into frozen soils. *Hydrological Processes*, *13*(12–13), 1827–1842. https://doi.org/10.1002/(SICI)1099-1085(199909)13:12/13<1827::AID-HYP896>3.0.CO;2-D

**How to cite this article:** LE Stone, Fang X, Haynes KM, et al. Modelling the effects of permafrost loss on discharge from a wetland-dominated, discontinuous permafrost basin. *Hydrological Processes*. 2019;33:2607–2626. https://doi.org/10.1002/hyp.13546